AD NUMBER

AD095491

NEW LIMITATION CHANGE

TO

Approved for public release, distribution unlimited

FROM

Distribution authorized to U.S. Gov't. agencies and their contractors; Administrative/Operational Use; 30 Jan 1956. Other requests shall be referred to Office of Naval Research, Arlington, VA.

AUTHORITY

ONR ltr, 9 Nov 1977

AFSWP 206, 716

Surface Temperatures in a Two-Layer Air-Spaced Slab System Irradiated from One Side

Technical Report No. 4

from

Fuels Research Laboratory
Massachusetts Institute of Technology
Cambridge, Massachusetts

Project DIC 6797

Prepared by: E. Ho Leong
M. E. Williams

Approved by: G. C. Williams

Contract N5-ori-07851
Office of Naval Research
Navy Department

Jan. 30, 1956

TABLE OF CONTENTS

Summary

A mathematical analysis has been carried out for unsteady state heat conduction through a simple two layer system consisting of a thin layer of material (cloth) at various distances from a semi-infinite solid (skin) shown in Fig. I and the temperature variations with time at various points on the system have been obtained by solving the appropriate heat flow equations. Curves have been drawn for different spacings between the cloth and main body and also for different spacings between the cloth and main body and also for different (thermal conductivity)(volumetric heat capacity) ratios $(kc\rho)_m/(kc\rho)_c$, where subscripts m and c refer to main body and cloth respectively.

Experiments were designed to determine whether the model shown in Fig. I was amenable to the mathematical analysis. The model consisted of cotton sateen over a polyethylene block (main body) and separated from it by an air space of known thickness. Temperature vs. time relationships were measured for the front and back cloth surfaces and thepolyethylene surface by irradiating the model on a solar furnace.

The results obtained were lacking somewhat in their reproducibility and in general the correlation between the theoretical and experimental curves was not very good. It is strongly believed that the moisture of the cloth is liberated in an explosive manner which complicates the mechanism of simple heat conduction. Various avenues exist for surmounting this difficulty. One method is to enclose the sample in a constant humidity container attached to the solar furnace with a shutter which opens simultaneously with the shutter of the furnace. Another method is to study the vapor loss as a function of time from a piece of fabric originally conditioned in an atmosphere of saturated water vapor. It would then be possible to know the water content of each fabric at the time it is irradiated

if it was pretreated in a saturated atmosphere. The latter approach will be used first.

Work on the development of a skin simulant with a "stretch factor" has been completed and will be used in future runs. This skin simulant, it is believed, will be able to simulate temperatures of the skin (when irradiated) at various "stretched" depths equivalent to smaller depths in the skin.

Introduction

The study of damage suffered by human skin when exposed to high intensity radiant heat fluxes liberated by an atomic explosion is of considerable importance. In particular, it is very important to be able to evaluate to what extent clothing materials are of practical utility in protecting skin. This report discusses in detail 1) the approach used in studying this problem and points out the controlling variables which determine the value of a piece of clothing material as a protective barrier against high intensity thermal radiation, 2) the techniques employed in studying this problem.

The problem of measuring the degree of damage suffered by organic materials such as human skin is in itself complex and not well understood at the present. Accelerated chemical decomposition and liberation of water, moisture and other volatile components are known to occur when the temperature of organic materials is raised high above normal temperatures. A direct measure might be a complete chemical analysis of the material before and after irradiation. Such a procedure is unduly complicated and unsuitable for the present project.

The second approach is to measure the temperature history of an irradiated skin. Evidences indicate that the degree of damage of organic materials is a function of the combined effects of the temperature level to which the material is raised and the duration this temperature level is maintained (7). Consequently the temperature history of the irradiated sample may be used as a measure of the degree of damage suffered. Comparison of the temperature histories of bare skin with that of skin protected by clothing will then serve as an indication of the value of clothing as a protective material.

The availability of live skin for experimentation purposes poses a problem, and it is necessary to find a skin simulant which when irradiated will behave

in a manner which corresponds to human skin in so far as temperature rises are concerned. A discussion of the theoretical considerations is presented which forms the basis for the skin simulant recently developed on this project.

The simplest idealization of a system composed of a human body protected by clothing material and which is susceptible to mathematical analysis is the two layer system shown in Fig. I. The cover represents the clothing material and the body is represented by the main body. The problem at hand is to establish a relationship of temperature vs. time at various positions of the system when a heat pulse ($I \propto \theta$) is impinged on the surface of the cover, (see Table of Nomenclature for symbols) and to test these relationships experimentally.

Theory

Unsteady State Heat Conduction

System of Equations

The time variation of the temperatures at various points of the system of Fig. I is obtained by solving the appropriate heat flow equations. In order to simplify the mathematics the following assumptions will be made:

a) Heat flow only in the -x- direction i.e., the y and z directions are infinite with uniform radiation striking the surface of the cover.

b) The cover may be thought of as an opaque uniform solid with an apparent thickness x_c, apparent specific heat C_c, apparent density ρ_c, and absorptivity α_r which remains constant during irradiation.

c) The same assumptions are made for the main body as for the cover, with the exception of thickness which is assumed to extend infinitely back in the x direction (subscript m refers to main body).

d) Heat losses from the front surface of the cover by convection and reradiation may be characterized by a single heat transfer coefficient U_o.

e) Heat transfer from cover to main body through air gap may be characterized by a similar heat transfer coefficient U_i.

b) and c) contains the assumption of absence of chemical reaction during irradiation.

The following equations can be written with the above mentioned assumptions in mind:

$$\alpha_c \left.\frac{\partial^2 t}{\partial x^2}\right]_{cover} = \left.\frac{\partial t}{\partial \theta}\right]_{cover} \qquad (1a)$$

$$\alpha_m \left.\frac{\partial^2 t}{\partial x^2}\right]_{m} = \left.\frac{\partial t}{\partial \theta}\right]_{m} \qquad (2b)$$

which are simply the Fourier heat-conduction equations for the two layers. The approximate boundary conditions for these equations are

$$I\alpha_r - U_o\left(t_{x_c=0} - t_{surr.}\right) = -k_c \left.\frac{\partial t}{\partial x_c}\right]_{x_c} = 0 \qquad (3a)$$

for the front surface of the cover; and

$$-k_c \left.\frac{\partial t}{\partial x_c}\right]_{x_c=0} = U_i\left(t_{x_c=L_c} - t_{x_m=0}\right) = -k_m \left.\frac{\partial t}{\partial x_m}\right]_{x_m=0} \qquad (4a)$$

as the relationship between the back surface of the cover and the front surface of the main body. Equation (4a) contains the assumption of zero heat storage in the air gap.

Equations (1a) and (2a) form a system of simultaneous partial differential equations with non-linear boundary conditions (3a) and (4a). An expedient through laborious technique of solving these equations is by the Schmidt method of finite difference approximations.

It is desirable, at this point, to convert Equations (1a) to (4a) into dimensionless forms, which serve to generalize the numerical solutions. The conversion of the four equations to dimensionless form will be carried out for the sake of clarity and at the same time to point out the technique of this conversion. Multiplying both sides of Equation (1a) by the factor $\left(\frac{k_c}{I\alpha_r L_c}\right)\Big/\left(\frac{1}{L_c}\right)^2$ yields:

$$\frac{\left(\frac{\partial^2 t}{\partial x^2}\right)\left(\frac{k_c}{I\alpha_r L_c}\right)}{\left(\frac{1}{L_c}\right)^2} = \frac{\left(\frac{\partial t}{\partial \theta}\right)\left(\frac{k_c}{I\alpha_r L_c}\right)}{\left(\frac{1}{L_c}\right)^2} \cdot \frac{1}{\alpha_c}$$

Insertion of all quantities under the differential sign and observing the rules of partial differentiation gives as a final result:

$$\frac{\partial^2\left[\frac{t k_c}{I\alpha_r L_c}\right]}{\left[\frac{x_c}{L_c}\right]^2} = \frac{\partial\left[\frac{t k_c}{I\alpha_r L_c}\right]}{\left[\frac{\alpha_c \theta}{L_c^2}\right]} \qquad (1)$$

Similarly, Equation (2a) is converted to

$$\frac{\partial^2\left[\frac{t\,k_c}{I\alpha_r L_c}\right]}{\partial\left[\frac{x_m}{L_c}\right]^2} = \frac{\partial\left[\frac{t\,k_c}{I\alpha_r L_c}\right]}{\partial\left[\frac{\alpha_m \theta}{L_c^2}\right]} \qquad (2b)$$

It is advisable to express (2b) in a slightly different form by multiplying both sides of the equation by $1/\left(\frac{k_c}{k_m}\right)^2$:

$$\frac{\partial^2\left[\frac{t\,k_c}{I\alpha_r L_c}\right]}{\partial\left[\frac{x_m}{L_c}\cdot\frac{k_c}{k_m}\right]} = \frac{\partial\left[\frac{t\,k_c}{I\alpha_r L_c}\right]}{\partial\left[\frac{\alpha_m \theta}{L_c}\left(\frac{k_c}{k_m}\right)^2\right]} \qquad (2)$$

The reason for this alteration will become clear later.

The dimensionless forms of (3a) and (4a) are obtained in identical manner and the final results are:

$$\left.\frac{\partial\left[\frac{t\,k_c}{I\alpha_r L_c}\right]}{\partial\left(\frac{x_c}{L_c}\right)}\right]_{x_c=0} = -\left\{\frac{\left(\frac{k_c}{U_0 L_c}\right)-\left[\left(\frac{t\,k_c}{I\alpha_r L_c}\right)_{x_c=0}-\left(\frac{t\,k_c}{I\alpha_r L_c}\right)_{surr}\right]}{\left(\frac{k_c}{U_0 L_c}\right)}\right\} \qquad (3)$$

$$-\left.\frac{\partial\left[\frac{t\,k_c}{I\alpha_r L_c}\right]}{\partial\left(\frac{x_c}{L_c}\right)}\right]_{x_c=L_c} = \frac{\left(\frac{t\,k_c}{I\alpha_r L_c}\right)_{x_c=L_c}-\left(\frac{t\,k_c}{I\alpha_r L_c}\right)_{x_m=0}}{\left(\frac{k_c}{U_i L_c}\right)} = -\left.\frac{\partial\left[\frac{t\,k_c}{I\alpha_r L_c}\right]}{\partial\left[\frac{x_m}{L_c}\cdot\frac{k_c}{k_m}\right]}\right]_{x_m=0} \qquad (4)$$

Throughout these equations the temperature is measured by the quantity $\left(\frac{t\,k_c}{I\alpha L_c}\right)$; the position by $\left(\frac{x_c}{L_c}\right)$ and $\left(\frac{x_m}{L_c}\cdot\frac{k_c}{k_m}\right)$ in the cover and main body respectively. For the sake of brevity, these dimensionless variables will be replaced by the symbols as defined in Table I.

Table I

Dimensionless Quantity	Symbol
$\frac{t\ k_c}{I\ \alpha_r L_c}$	T
$\frac{x_c}{L_c}$	X_c
$\frac{x_m}{L_c} \cdot \frac{k_c}{k_m}$	X
$\frac{\alpha_c\ \theta}{L_c^2}$	Θ_c
$\frac{\alpha_m\ \theta}{L_c^2} \cdot \left(\frac{k_c}{k_m}\right)^2$	Θ_m

The advantage of using the dimensionless parameters $\frac{x_c}{L_c}$ and $\frac{x_m}{L_c} \cdot \frac{k_c}{k_m}$ as a measure of distance is indicated by Equation (4). This states that the dimensionless temperature gradient at $x_c = L_c$ and $x_m = 0$ are numerically equal. Furthermore, this gradient is numerically equal to the slope of a line of height $\left(\frac{t\ k_c}{I \alpha_r L_c}\right)_{x_c = L_c} - \left(\frac{t\ k_c}{I \alpha_r L_c}\right)_{x_m = 0}$ and distance of $\frac{k_c}{U_i L_c}$.

Method of Finite Difference Approximations

a) General Equations:

Equations (1) to (4) can be written in the finite difference form by transforming the differentials to finite increments. For example, differential dimensionless temperature gradient is written as:

$$\frac{\partial T}{\partial X_c} = \frac{\Delta_x (T)}{\Delta (X_c)}$$

and

$$\frac{\partial T}{\partial X_m} = \frac{\Delta_x T}{\Delta (X_m)}$$

the second partial derivatives with respect to x may be written as:

$$\frac{\partial^2 [T]}{\partial [X_c]^2} = \frac{\Delta_x [\Delta_x (T)]}{\Delta [X_c]^2}$$

and

$$\frac{\partial^2 [T]}{\partial [X_m]^2} = \frac{\Delta_x [\Delta_x (T)]}{\Delta [X_m]^2}$$

The time derivatives are similarly written as:

$$\frac{\partial (T)}{\partial (\Theta_c)} = \frac{\Delta_\theta [T]}{\Delta (\Theta_c)}$$

and

$$\frac{\partial (T)}{\partial (\Theta_m)} = \frac{\Delta_\theta [T]}{\Delta [\Theta_m]}$$

Throughout these equations, Δ_x refers to partial differentiations with respect to x and Δ_θ refers to partial differentiation with respect to θ .

In finite difference form, Equations (1) to (4) will appear as:

$$\frac{\Delta_x [\Delta_x (T)]}{\Delta [X_c]^2} = \frac{\Delta_\theta [T]}{\Delta [\Theta_c]} \qquad (5a)$$

$$\frac{\Delta_x [\Delta (T)]}{\Delta [X_m]^2} = \frac{\Delta_\theta [T]}{\Delta [\Theta_m]} \qquad (6a)$$

$$\left.\frac{\Delta_x (T)}{\Delta (X_c)}\right]_{x_c=0} = \left\{ \frac{\left(\frac{k_c}{U_0 L_c}\right) - \left(T_{x_c=0} - T_{surr}\right)}{\left(\frac{k_c}{U_0 L_c}\right)} \right\} \qquad (7)$$

$$\left.\frac{\Delta_x (T)}{\Delta (X_c)}\right]_{x_c=L_c} = \frac{T_{x_c=L_c} - T_{x_m=0}}{\frac{k_c}{U_i L_c}} = \left.\frac{\Delta_x (T)}{\Delta (X_m)}\right]_{x_m=0} \qquad (8)$$

b) Schmidt Technique

As an illustration of finite difference approximations to the solutions of partial differential Equations (1) to (4), consider Fig. 2. The cover is divided by an integral number (n) of construction lines (shown dotted) equally spaced from each other. In Fig. 2, n = 4 is used making

$$4\,\Delta (X_c) = \left(\frac{L_c}{L_c}\right) = 1 \; ; \quad \Delta (X_c) = \frac{1}{4}$$

The construction lines are placed such that half of a construction slab extends beyond the surfaces.

The main body construction lines are separated a distance $\Delta\left(\frac{x_m}{L_c} \cdot \frac{k_c}{k_m}\right)$ apart. This separation depends on $\Delta\left(\frac{x_c}{L_c}\right)$ as will be explained later; but for the

moment assume that the main body has been correctly divided. At any time after irradiation, the temperature profile in the two layers may be approximated by the solid line as shown. The degree of approximation depends on the fineness in which the layers are divided by the construction lines.

In terms of Fig. 2 then, Equation (5a) may be written as:

$$\left[T_{m\Delta x-1} - T_{m\Delta x}\right]_{n\Delta\theta} - \left[T_{m\Delta x} - T_{m\Delta x+1}\right]_{n\Delta\theta} = \frac{\left[T_{n\Delta\theta+1} - T_{n\Delta\theta}\right]_{m\Delta x}}{\Delta\theta_c} \cdot \Delta\left(X_c\right)^2 \qquad (5b)$$

Both the dimensionless distance and time are independent variables, and their choice is arbitrary for any particular series of calculations. The Schmidt method uses a value of:

$$\frac{\Delta\left(X_c\right)^2}{\Delta\left(\theta_c\right)} = 2 \qquad (9)$$

which introduces some simplifications in the numerical work. Combining (5b) and (9) gives:

$$T_{n\Delta\theta+1,\, m\Delta x} = T_{n\Delta\theta,\, m\Delta x} + \left[\frac{\Delta T_{m\Delta x-1} + \Delta T_{m\Delta x+1}}{2}\right]_{n\Delta\theta}$$

Equation (5) provides a rule for the numerical calculations. It enables the calculation of the temperature at time $n\Delta\theta+1$, from a knowledge of the temperature distribution at time $n\Delta\theta$.

Similarly, the corresponding equation for the main body temperatures is:

$$T_{n\Delta\theta+1,\, p\Delta x} = T_{n\Delta\theta,\, p\Delta x} + \left[\frac{T_{p\Delta x-1} + T_{p\Delta x+1}}{2}\right]_{n\Delta\theta}$$

if

$$\frac{\Delta\left(X_m\right)}{\Delta\left(\Theta_m\right)} = 2$$

The boundary condition (8) simply says that the dimensionless temperatures at planes (e) and (f) are determined by a straight line connecting the temperatures at plane (d) and (g), provided planes $x_c = L_c$ and $X_m = 0$ are separated by the distance $k_c / U_i L_c$.

Boundary condition (7) is satisfied by placing a construction point 0 at a distance $k_c/U_0 L_c$ to the left of plane $x_c = 0$ and $k_c/U_0 L_c$ above the initial temperature T_0. It is clear from Fig.2A that a straight line drawn from point 0 to the instantaneous temperature value of plane (b) will satisfy Equation (7). This determines the value of the temperature at plane (a).

The purpose of extending the construction lines to a half slab thickness is to obtain a better approximation to the actual situation. Notice that the surface temperature gradient, in this manner, only extends a half slab thick into the layers; while dividing the layer with the construction lines coincident with the surfaces result in extending this gradient one whole slab division into the layers.

Equation (7) provides the information that the mapping of the construction lines must be different for the two layers. However, an additional relationship is required to fix the ratio $\Delta X_c/\Delta X_m$, as an arbitrary choice of ΔX_c still leaves ΔX_m undetermined. Such a constraint is provided by Equations (9) and (10).

To insure the condition that a unit change of $\Delta \Theta_c$ and $\Delta \Theta_m$ will give exactly the same change of θ in terms of seconds, then combining (9) and (10) results in:

$$\frac{\Delta (X_c)^2}{\Delta \Theta_c} = \frac{\Delta (X_m)^2}{\Delta \Theta_m}$$

or

$$\frac{\Delta X_c}{\Delta X_m} = \sqrt{\frac{\alpha_c}{\alpha_m} \cdot \left(\frac{k_m}{k_c}\right)^2} = \sqrt{\frac{c_m \rho_m k_m}{c_c \rho_c k_c}}$$

Equation (11) provides the scaling factor for ΔX_m in terms of ΔX_c, when the thermal properties of the two materials are known. It is the result of the combined effects due to differences in thermal properties and the necessity of equalizing the time in the two layers. Notice that if the thermal properties are identical in the two layers, the construction lines are equally spaced in the two solids.

Theory of Skin Simulant

One of the difficulties involved in obtaining a system for skin simulant is finding a material which possesses the same conductivity, heat capacity and density as skin. A second difficulty arises when one attempts to measure temperatures at specific depths below the skin surface. The theoretical discussion which ensues describes a skin simulant which it is believed will satisfactorily embody the above requirements.

In a semi-infinite solid, heat transmission is determined by the unique groups $\Delta T\sqrt{kc\rho}/I\alpha t$ and $kt/c\rho x^2$ where ΔT represents temperature rise, k the thermal conductivity, t the time, and $c\rho$ the volumetric heat capacity, x the depth, and $I\alpha$ the absorbed-radiation intensity. Since $I\alpha$, t and ΔT are variables, the groups $kc\rho$ and $k/c\rho x^2$ should be the same in skin and simulant for proper modelling. With subscript s referring to simulant and sk for skin, it follows that $kc\rho)_s = kc\rho)_{sk}$ and $(k/c\rho x^2)_s = (k/c\rho x^2)_{sk}$. Furthermore:

$$\frac{x_s}{x_{sk}} = a = \sqrt{\frac{k_s}{k_{sk}} \cdot \frac{(c\rho)_{sk}}{(c\rho)_s}} = \sqrt{\frac{k_s}{k_{sk}} \cdot \frac{k_s}{k_{sk}}} = \frac{k_s}{k_{sk}}.$$

and the depth x, of a point in the simulant corresponding to one in the skin will be much greater if k_s is much larger and $c\rho)_s$ much smaller than k_{sk} and $c\rho)_{sk}$, respectively. Since such a material does not exist, a copper fin device has been adopted, consisting of 0.005" copper fins attached to a 0.002" copper sheet with 0.125" air spaces between the fins. The fins provide high conductivity and the 1/8" air spaces between them the low volumetric heat capacity. Thus if the total heat flow cross section of the fins is the fraction a times the area of the surface to which they are attached, then the effective bulk condictivity of the fin system is ak_{cu} and the effective bulk volume heat capacity is $a(c\rho)_{cu}$.

For the copper fins selected the ratio x_s/x_{sk} is 30/1 so that a system of fins 60 mm deep would correspond to 2 mm of flesh and thermocouples spaced at 6 to 10 mm intervals can readily be placed in the simulant.

Design and construction of the copper-fin skin simulant has taken place since the experiments reported here and no radiation tests with it have yet been made. The polyethylene simulant used in this work has thermal properties in the same order of magnitude as those of skin, as shown in the following tabulation (8):

Material	k $\frac{cal}{(cm)(sec)(^oC)}$	c $\frac{cal}{gm\,^oC}$	ρ $\frac{gm}{cc}$	$c\rho$	$kc\rho$	$k/c\rho$
Polyethylene	8.0×10^{-4}	0.55	0.92	0.506	4.05×10^{-4}	15.8×10^{-4}
Skin	10.6×10^{-4}			0.8	8.5×10^{-4}	13.3×10^{-4}

Equipment

The experimental investigations were carried out by the utilization of a solar furnace (2) as the source of high intensity thermal radiation. Intensities ranging up to 6.89 cal/cm^2 sec. were obtained during the summer months. The mirrors and some of the auxiliary equipment are housed in a steel-reinforced wooden structure and this structure is fixed on an altazimuth mount. The primary mirrors (3" x 3"), four hundred in all, which receive the direct radiation from the sun are located at the rear of the housing and they in turn reflect the sun's rays on a secondary mirror, which is trapezoidal in shape. The secondary mirror reflects the radiation to the target area where the sample to be radiated is placed.

The secondary mirror is located on a rotatable axis thus obviating the necessity of having the target area exposed to the radiation during the period before and after a run.

The shutter mechanism in the target area is operated by an automatic timer using solenoids as the initiating adjuncts. Two shutters are used during the operation, one exposing the sample to radiation, the second occluding radiation at the end of the desired pulse.

The total radiation is measured by an Eppley Pyrheliometer and continuously recorded by a Leeds and Northrup strip chart potentiometer. Blocking off the direct rays of the sun provides a measure of the diffuse radiation, and the difference between the total and the surrounding radiation is the focussable intensity on the primary mirrors of the furnace.

The sample models are composed basically of cotton sateen stretched over a circular polyethylene block. The cloth contains two silver-constantan thermocouples, one on each surface; a third thermocouple is located on the surface

of the polyethylene block. Other appurtenances to the models merely serve to hold the cloth and polyethylene in place and to provide electrical connection between the thermocouples and the temperature recording instruments. In the cases where studies were made with spacing between cloth and skin simulant, a metal ring of known thickness was inserted between the two.

Temperature readings of the thermocouples were recorded by a Heiland type photographic galvanometer.

The thermocouples were made from 0.001 inch constantan wire half of which was plated with silver from a A_gCN bath. Close contact between the thermocouple and the cloth was achieved by weaving the couples into the cloth surface. Contact between the polyethylene block and its thermocouple and the covering when no spacing was used was accomplished by machining a slight convex curvature in the surface of the polyethylene.

Procedure

Prior to the experimental runs, the samples were assembled, after which the resistances of the thermocouples were determined. It was necessary to determine the resistances of the couples and also the connecting lines since the recording galvanometer which was employed is a current-measuring instrument. The assembled sample was then placed in the sample holder at the target area and the thermocouple leads connected, after which the furnace was aligned to the sun and the secondary mirror rotated to direct the radiation to the sample. At this point the Heiland apparatus was set in motion. The shutter release also put the timer in simultaneous operation. At the end of a preset time the other shutter closed off the radiation automatically.

In order to get the total radiation, it is necessary to determine the furnace multiplier by means of a silver disc calorimeter. The calculation of this multiplier is included in the appendix.

Results

The results obtained from the irradiated samples are presented in Figures 3-18 showing the temperature-time histories of the three surfaces mentioned. The temperature and time scales are given in dimensionless groups in Figs. 3-10 and in Figs. 11-18 the temperature and time scales are in terms of degrees centigrade and seconds respectively. For the purpose of observing the effects of spacing the plots have been made (Figs. 3-10) for the same color fabric. Theoretical temperature-time histories are shown in Figs. 19-36, in the Appendix.

It should be mentioned that the transmissivity of the fabrics varies for each color; the light colors have the largest values, while for black it is practically zero. These values together with the absorptivity constants were obtained from the University of Rochester (3). A brief glance at Table 3 shows that temperature rise due to direct transmission of heat through the cloths can constitute a large percent of the total temperature rise for surfaces covered with these cloths.

Discussion of Results

A comparison of the predicted curves and the experimental curves reveals much discrepancy for the cloth top and under surface (Fig. 3.) However, the correlation between the theoretical and experimental curves for the polyethylene surface is fairly good.

The slopes of the experimental curves for the top surfaces are much lower than the predicted slopes with the exception of the white fabric which was the only sample which fits the theoretical slope. The value of the absorptivity used for white cloth was 0.093; a value of 0.12 would give a correlation more consistent with the other samples, as shown by Figure 3A.

It was suspected that perhaps a difference between the spectra of the sun and the carbon arc source could cause different absorptivity values, since the latter source was employed in determining absorptivity values, but a comparison of these two spectra showed no important differences.

The smaller slopes of the cloth top surface appear to be the result of a heat absorption by the inherent moisture content of the fabric. This moisture would tend to increase the conductivity of the air gap between the cloth and polyethylene surface than would be expected (Fig. 3).

The curves whose coordinates are in terms of degrees and seconds show the effect of color on the temperature rise. The darker shades with higher absorptivity give a steeper and higher temperature rise, than the light shades (Figs. 11-18).

It is interesting to note that although the theory predicted a very small difference in the slopes and temperature rise for the polyethylene surface temperatures for 0.32 and 0.51 cm spacings, in the actual results the difference was greater than expected. The mechanism whereby this difference came about

is, in the absence of some means of direct observation, largely a matter of conjecture. It can be seen that the temperature rise for the cloth back surface is instantaneous while for plain heat conduction there is quite a lag. This deviation suggests that heat transfer to the back surface is also by means of conduction and by other means, probably steam and/or direct radiation. However no correction was made for this in the theory.

From the foregoing discussion it is apparent that the moisture associated with the cloth is a variable hitherto unaccounted for, and apart from complicating the mechanism of heat transfer, has also prevented reproducibility of results because the moisture content of the fabric at any moment depends on the humidity of the ambient air. Preliminary studies have been carried out on the rate of moisture loss from pieces of the fabric which were immersed in an atmosphere saturated with water vapor. The results show that it requires approximately 10 minutes in quiescent air for the cloth to be reduced to 1/e of its original water content. This information will be useful in future work in knowing the water content of the cloth samples irradiated.

Conclusions

The simple treatment of heat conduction through a two layer system is inadequate to describe the heat transfer process through the model described. This process is apparently complicated by the presence of moisture in the cloth layer. However, the results do indicate that the lighter-shade fabrics give better protection from radiation damage than dark ones do, over the first two seconds after exposure.

Future Work and Recommendations

For future work it is recommended that:

1. The cloth samples be pretreated in a saturated atmosphere of water vapor before irradiation. Application of the rate of loss of water vapor in air should indicate the amount present at the time of irradiation, provided that the cloth is properly protected from air currents.

2. The surface of the skin simulant developed will be blackened with a non-lustrous thin coating and the simulant's performance will be compared with semi-infinite solid theory and with data obtained by other investigations.

3. The skin simulant with cloth coverings will then be irradiated.

4. If reproducibility is still unobtainable due to inability to know the cloth moisture with sufficient accuracy, then it is suggested that a constant humidity device be developed which is attachable to the furnace with a shutter mechanism of the furnace.

APPENDIX

Nomenclature

c = Heat capacity $\frac{cal}{gm^{\circ}C}$

I = Intensity of Radiation $\frac{cal}{cm^2 - sec}$

k = Conductivity $\frac{cal}{cm\ sec\ ^{\circ}C}$

L = Thickness of cloth. cm

t = Temperature $^{\circ}C$.

Δt = Temperature rise ($^{\circ}C$)

T = Dimensionless temperature rise $\frac{\Delta t\ k\ c}{I\ L_c \alpha_\gamma}$ (α_γ = absorptivity)

U = Heat Transfer coefficient $\frac{cal}{cm^2\ sec\ ^{\circ}C}$

Greek

α = $\frac{k}{c\rho}$

ρ = Density $\frac{gm}{cm^3}$

θ = Dimensionless time $\frac{\alpha\theta}{L_c^2}$

τ = Transmissivity

Subscript

c refers to cloth

m refers to polyethylene

Bibliography

(1) Carslaw, H. S., and Jaeger, J. C.,"Conduction of Heat in Solids", Oxford, N. Y., 1947.

(2) Gardon, R.,"Temperature Attained in Wood Exposed to High Intensity Thermal Radiation", Technical Report No. 3, D.I.C. Project 6797, Fuels Research Laboratory, M.I.T. Cambridge, Mass.

(3) Krolak, L. J., Davis, T. P., "The Measurement of Diffuse Reflectance of Cloths and Skin Samples", The University of Rochester Atomic Energy Report UR-380 (1955).

(4) McAdams, W. H., "Heat Transmission", Hottel Charts, Figs. 3-4, McGraw Hill, N. Y. 1954.

(5) Mickley, H. S., "The Numerical Solution of Partial Differential Equations", Notes for Department of Chem. Eng., M.I.T. 1953.

(6) Sherwood, T. K. and Reed, C. E., "Applied Mathematics in Chem. Eng.", McGraw Hill, N. Y. 1939.

(7) Williams, C. C., "Damage Initiation in Organic Materials Exposed to High-Intensity Thermal Radiations", Sc. D. Thesis in Chem. Eng., 1953.

(8) Derksen, W. L., Bates, W. J. and Monahan, T. I., Final Report, NS-081-001, On the Use of Polyethylene as a Physical System for Evaluating Physiological Burns Behind Fabrics; Naval Material Laboratory Project 5046-3, Part 42; AFSWP 834; New York Naval Shipyard, Brooklyn, N. Y., November 1954.

Sample Calculation of Run

$E.M.F._{direct} = (E.M.F._{total} - E.M.F._{indirect}) = (0.857 - 0.105)4$

$= 3.01$ mv

Sensitivity of pyrheliometer = 2.45 mv/cal/min cm^2

Time = D.S.T. - 1:00 + (Corr. for eq. of time + corr. for longitude) =

(11:43 - 1:00) + 0.19 = 11.02

From plot of Cos θ vs Time: Cos θ = 0.860 (corres. to 11:02 A.M.)

$$I \text{ (radiant intensity)} = \frac{3.01 \times 289}{2.45 \times 0.86} = 6.89 \text{ cal/cm}^2 \text{ sec.}$$

where furnace const = 289.

Temperature-Time Calculations

Galvanometer Deflections = Y cm

Sensitivity of Galvanometer = 12.25 cm/m.a.

Thermocouple + Line resistances = 47.6 ohms

$$E.M.F. = \frac{Y}{12.25} \times 47.6 = 3.72\ Y$$

Substitution of values of Y at corresponding times X gives the temperature-time history.

Furnace Multiplier by Means of Silver Disc Calorimeter

Observed Rate of Temperature Rise = 39.6° C/sec.

Cooling Correction = 2.8° C/sec.

Corrected Rate of Temp. Rise = 42.4° C/sec.

Calorimeter Constant = 0.151 cal/°C cm^2

Radiant Intensity at Target = 42.5 x 0.151 cal/cm^2 sec.

= 6.40 cal/cm^2 sec.

Furnace Multiplier cont'd

Solar Intensity

E.M.F. = $(E.M.F._{total} - E.M.F._{indirect})$ = (0.79 - 0.11)4

= 2.72 mv.

Sensitivity of Pyrheliometer = 2.45 mv/cal cm^2 min.

Solar Time = D.S.T. - 1:00 + (corr. for eq. of time and longitude)

= 2:15 - 1:00 + 0.19.4 = 1:34

Cos θ = 0.86 (corres. to 1:34)

$$I = \frac{2.72}{2.45 \times 0.86} = 1.29 \text{ cal/min cm}^2$$

$$\text{Multiplier} = \frac{6.40 \times 60}{1.29} = 298$$

Several runs yielded an average multiplier of 289.

Temperature Rise due to Transmittance

Equation for temperature rise on the surface of a semi-infinite solid when irradiated is given by:

$$\frac{\Delta T \sqrt{kc\rho}}{I\tau\sqrt{t}} = \frac{2}{\sqrt{\pi}}$$ (ref. 1, p11, eq. 1.10)

Polyethylene Properties

$\sqrt{kc\rho}$ = $\sqrt{15.8 \times 10^{-4}}$ = 3.99×10^{-2}

t = 0.238 sec. (time interval)

Cloth Properties

Transmissivity (τ)

White	0.1610	D. Gray	0.00
L. Gray	0.0611	Black	0.00
M. Gray	0.010		

$$\Delta T = \frac{2 \times I\tau\sqrt{t}}{\sqrt{kc\rho}} = 28.3 \ (I\tau)\sqrt{t} \ (^{\circ}C)$$

For results see Table III.

TABLE II

Theoretical Temperature Rise of Polyethylene Surface Due to Cloth Conduction (°C); $\frac{U_o L_c}{k_c}^{*} = 0.1$

Time Intervals		Cloth Color and Radiation Intensity: cal/(sec)(cm)^2		
Sec.	Dimensionless $\frac{\alpha_c \theta}{L_c^2}$	White I=5.74	Light Gray I=6.65	Medium Gray I=5.74
			Spacing = 0 cm	
0	0	0	0	0
0.238	0.0312	0	0	0
0.476	0.0624	0	0	0
0.714	0.0936	0.78	3.89	5.98
0.952	0.1248	1.16	5.83	8.97
1.190	0.1560	1.94	9.72	15.0
			Spacing = 0.32 cm	
0	0	0	0	0
0.238	0.0312	0	0	0
0.476	0.0624	0	0	0
0.714	0.0936	0	0	0
0.952	0.1248	0	0	0
1.190	0.1560	0.02	0.09	0.14
			Spacing = 0.51 cm	
0	0	0	0	0
0.238	0.0312	0	0	0
0.476	0.0624	0	0	0
0.714	0.0936	0	0	0
0.952	0.1248	0	0	0
1.190	0.1560	0.01	0.06	0.09

* Ratio of convection (to surroundings) to conduction rate (into sample).

TABLE III

Theoretical Temperature Rise of Polyethylene Surface

Due to Transmittance through Cloth (°C)

	Cloth Color, Radiation Intensity, I, and Transmittance, τ		
Time (secs)	White	Light Gray	Medium Gray
	I = 5.74	I = 6.68	I = 5.74
	τ = 0.161	τ = 0.061	τ = 0.010
0.238	12.8	5.64	.806
0.476	18.1	7.98	1.14
0.714	22.4	9.87	1.42
0.952	25.6	13.4	1.62
1.190	28.6	15.0	1.81

TABLE IV

Theoretical Temperature Rise of Polyethylene Surface

Due to Transmittance and Conduction (°C)

Time Intervals		Cloth Color and Radiation Intensity cal/(sec)(cm)^2		
Sec	Dimensionless $\frac{\alpha_c \theta}{L_c^2}$	White I=5.74	Light Gray I=6.65	Medium Gray I=5.74
		Spacing = 0 cm		
0	0	0	0	0
0.238	0.0312	12.8	5.64	0.81
0.476	0.0624	18.1	7.98	1.14
0.714	0.0936	23.18	13.76	7.40
0.952	0.1248	26.76	23.12	10.59
1.190	0.1560	30.55	30.61	16.90
		Spacing = 0.32 cm		
0	0	0	0	0
0.238	0.0312	12.8	5.64	0.806
0.476	0.0624	18.1	7.98	1.14
0.714	0.0936	22.4	9.87	1.42
0.952	0.1248	25.6	13.4	1.62
1.190	0.1560	28.62	15.09	1.95
		Spacing = 0.51 cm		
0	0	0	0	0
0.238	0.0312	12.8	5.64	0.806
0.476	0.0624	18.1	7.98	1.14
0.714	0.0936	22.4	9.87	1.42
0.952	0.1248	25.6	13.4	1.62
1.190	0.1560	28.61	15.06	1.90

Fig. 1

TWO-LAYER SYSTEM

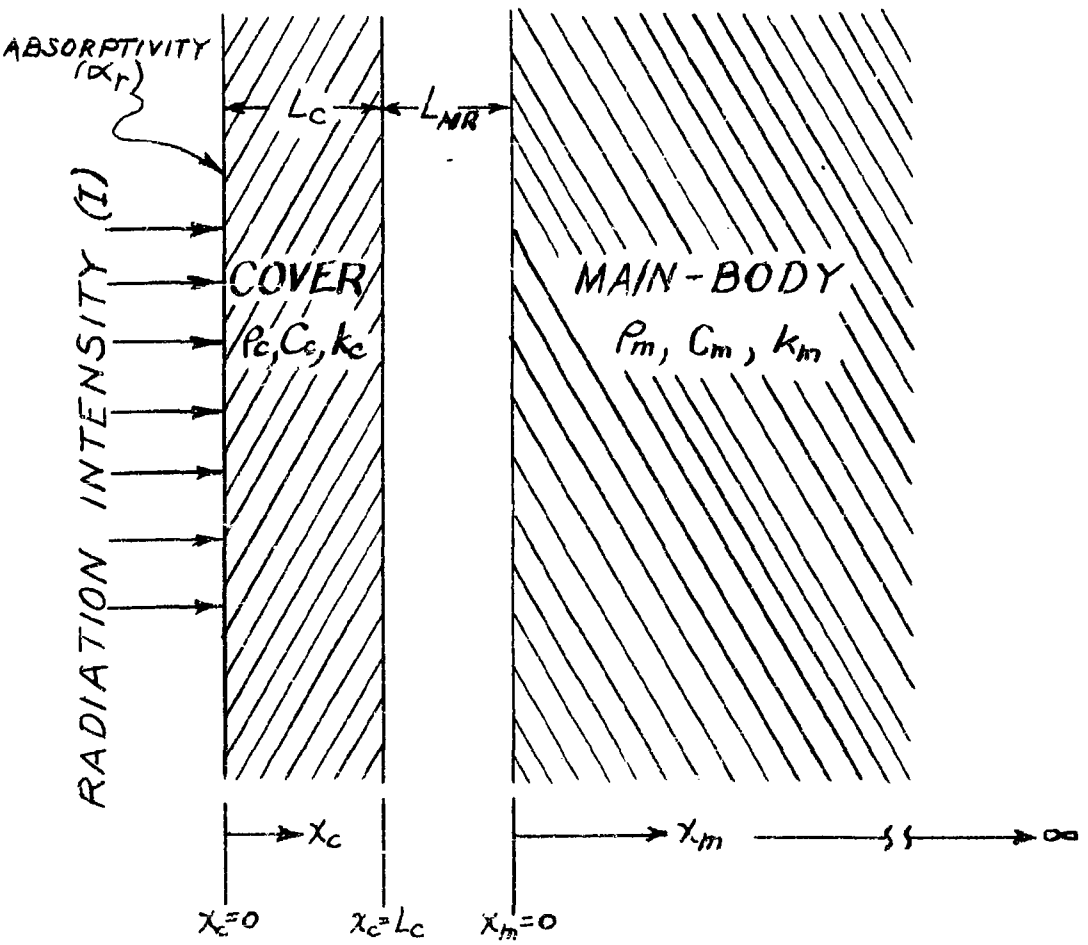

Fig. 2

GRAPHICAL SCHMIDT TECHNIQUE

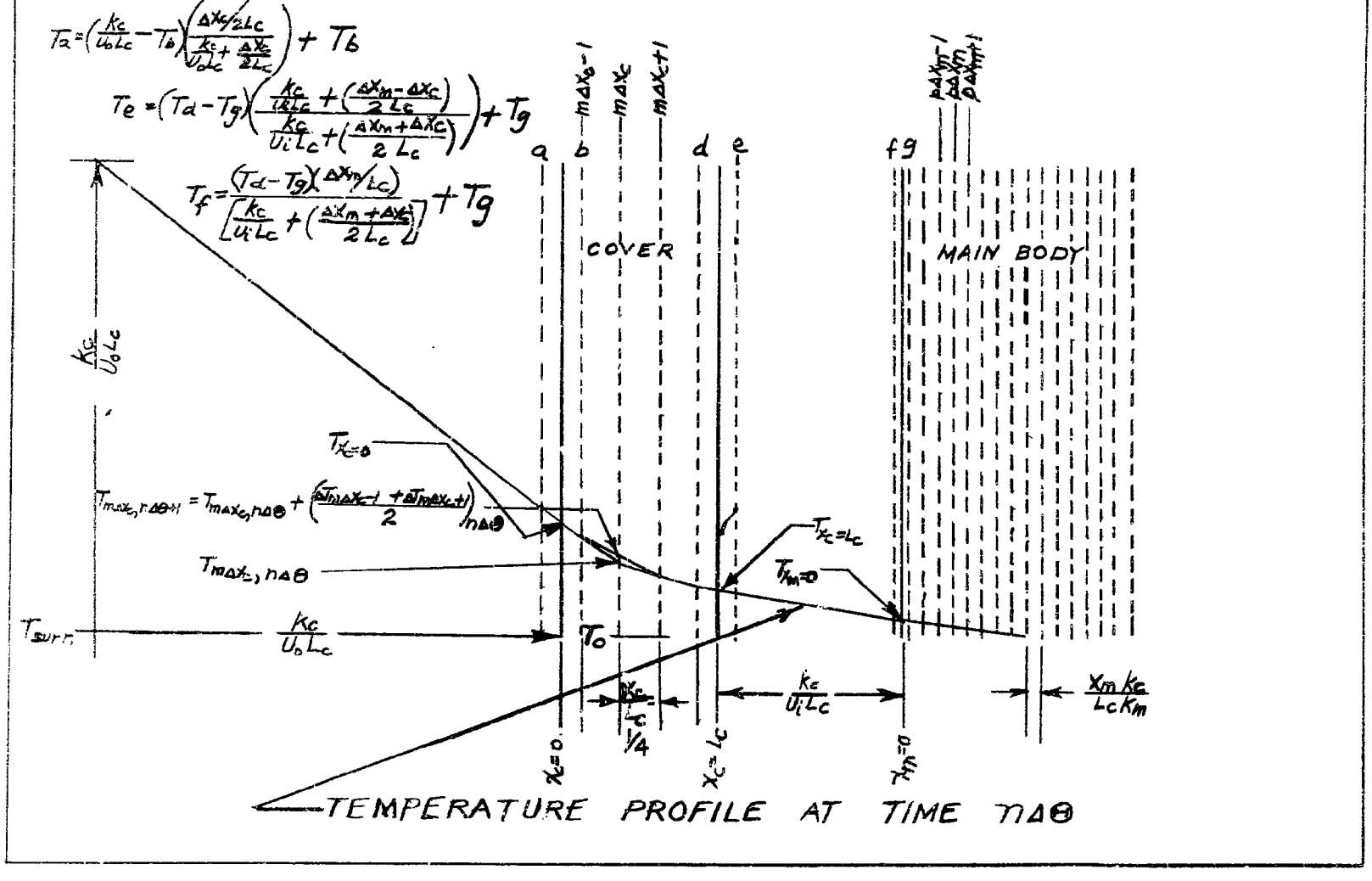

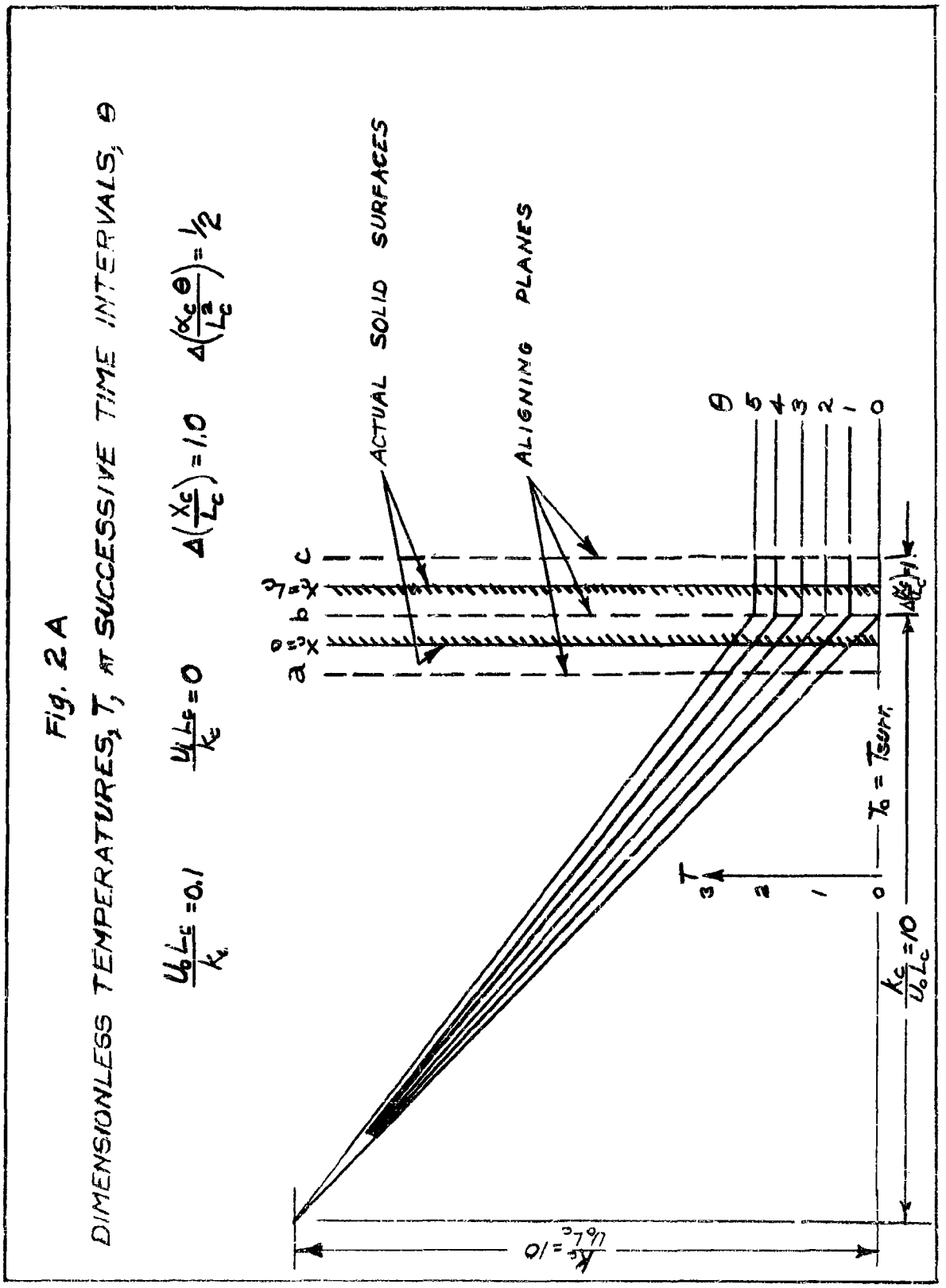
Fig. 2A
DIMENSIONLESS TEMPERATURES, T, AT SUCCESSIVE TIME INTERVALS, θ
$\frac{U_0 L_c}{k_c} = 0.1$
$\frac{U_0 L_c}{k_c} = 0$
$\Delta\left(\frac{x_c}{L_c}\right) = 1.0$
$\Delta\left(\frac{\alpha_c \theta}{L_c^2}\right) = 1/2$
ACTUAL SOLID SURFACES
ALIGNING PLANES
θ 5 4 3 2 1 0
a x=0 b y=x c
T 3 2 1 0
T0 = Tsurr.
$\frac{k_c}{U_0 L_c} = 10$

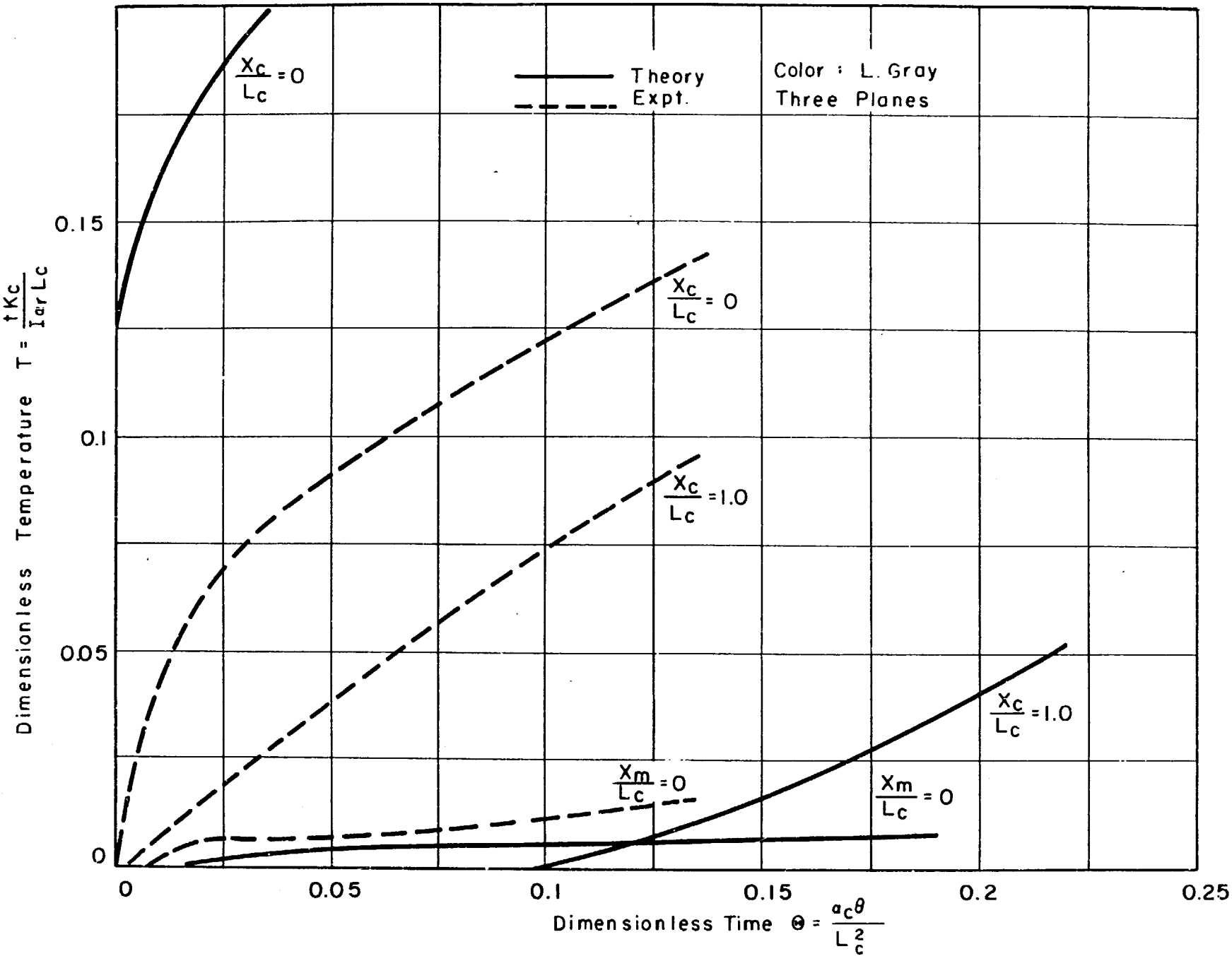

FIG. 3 COMPARISON OF THEORY & EXPT.

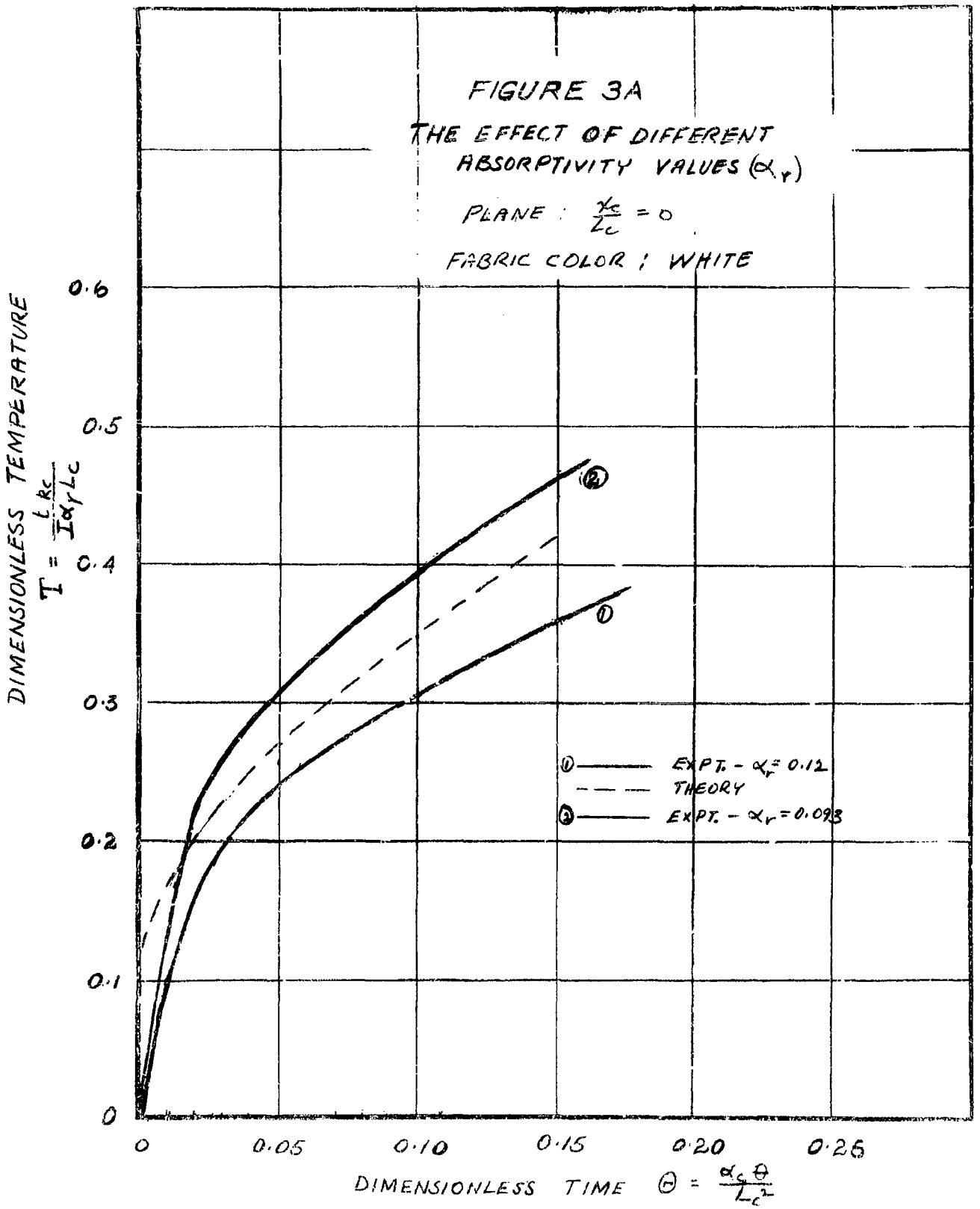
FIGURE 3A
THE EFFECT OF DIFFERENT ABSORPTIVITY VALUES (α_r)
PLANE : $\frac{x_c}{L_c} = 0$
FABRIC COLOR : WHITE
DIMENSIONLESS TEMPERATURE $T = \frac{t\,k_c}{I \alpha_r L_c}$
0.6
0.5
0.4
0.3
0.2
0.1
0
0
0.05
0.10
0.15
0.20
0.25
DIMENSIONLESS TIME $\Theta = \frac{\alpha_c \theta}{L_c^2}$
① EXPT. - $\alpha_r = 0.12$
THEORY
② EXPT. - $\alpha_r = 0.093$

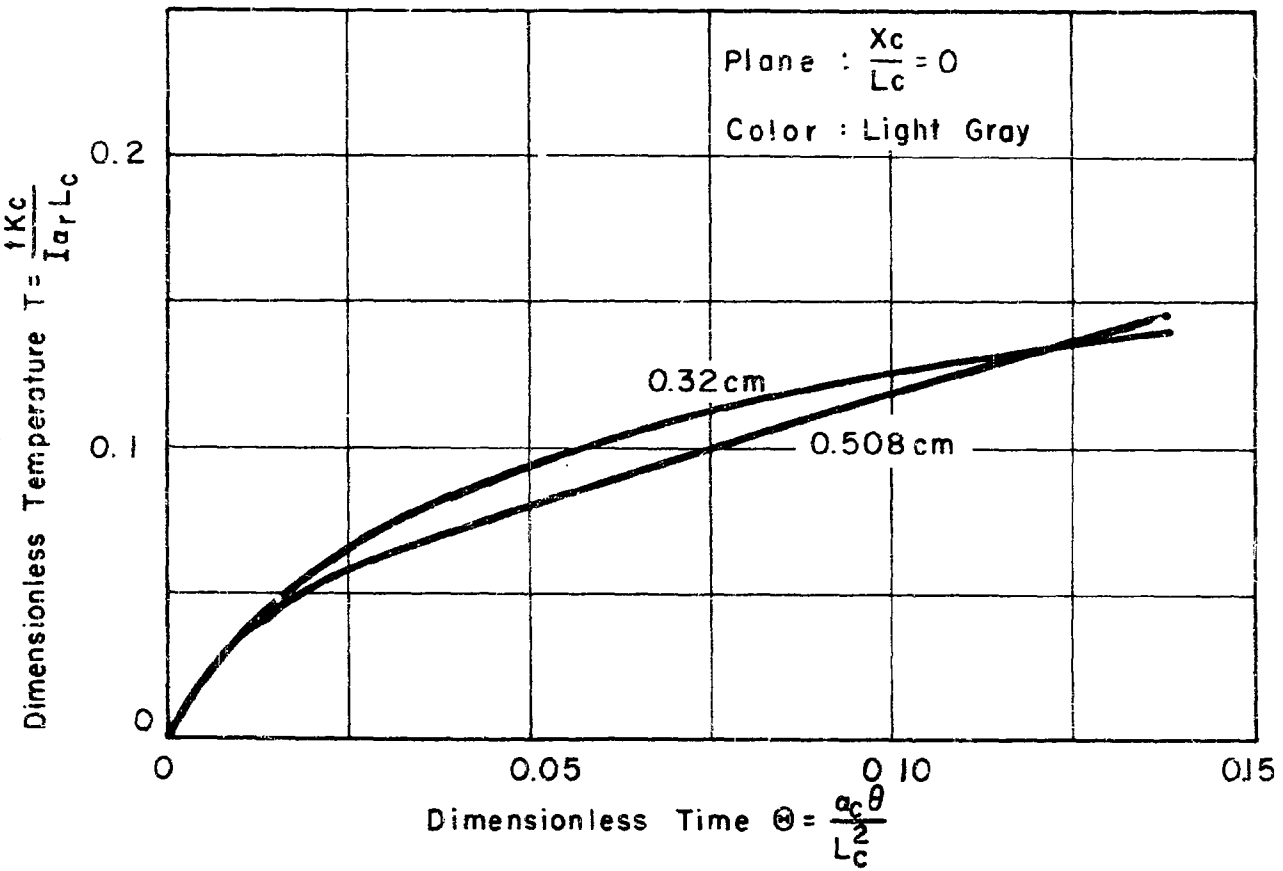

FIG. 4 SPACING EFFECTS

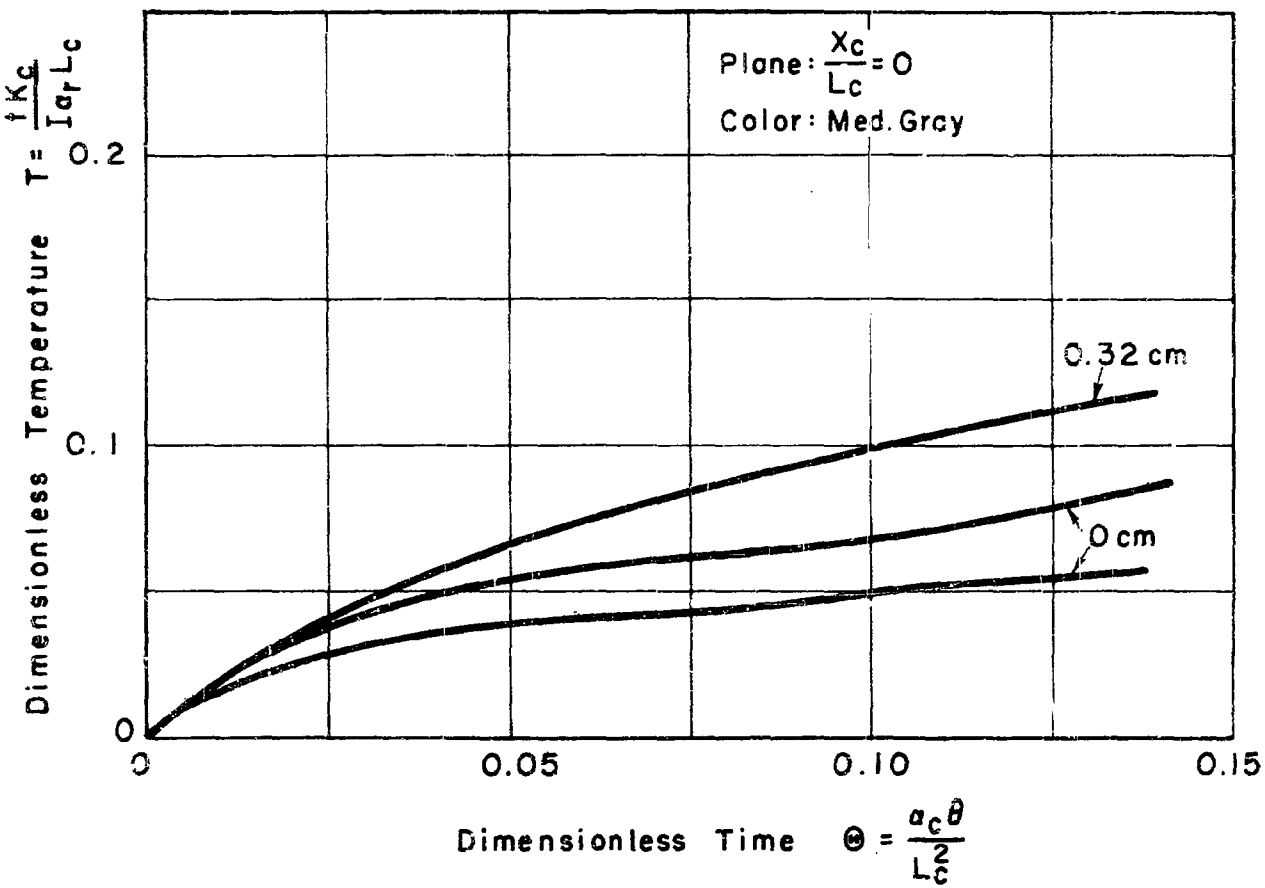

FIG. 5 SPACING EFFECTS

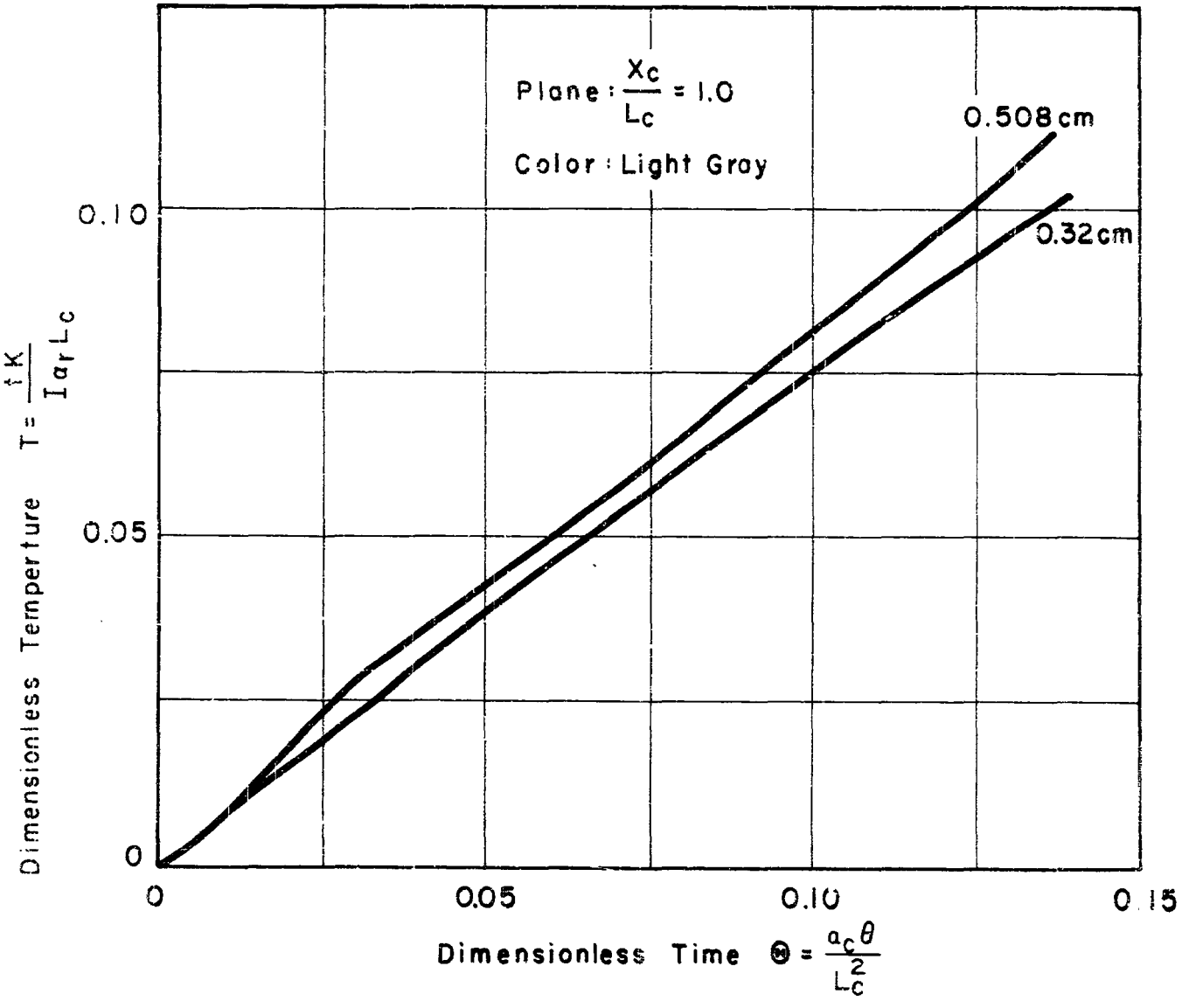

FIG. 6 SPACING EFFECTS

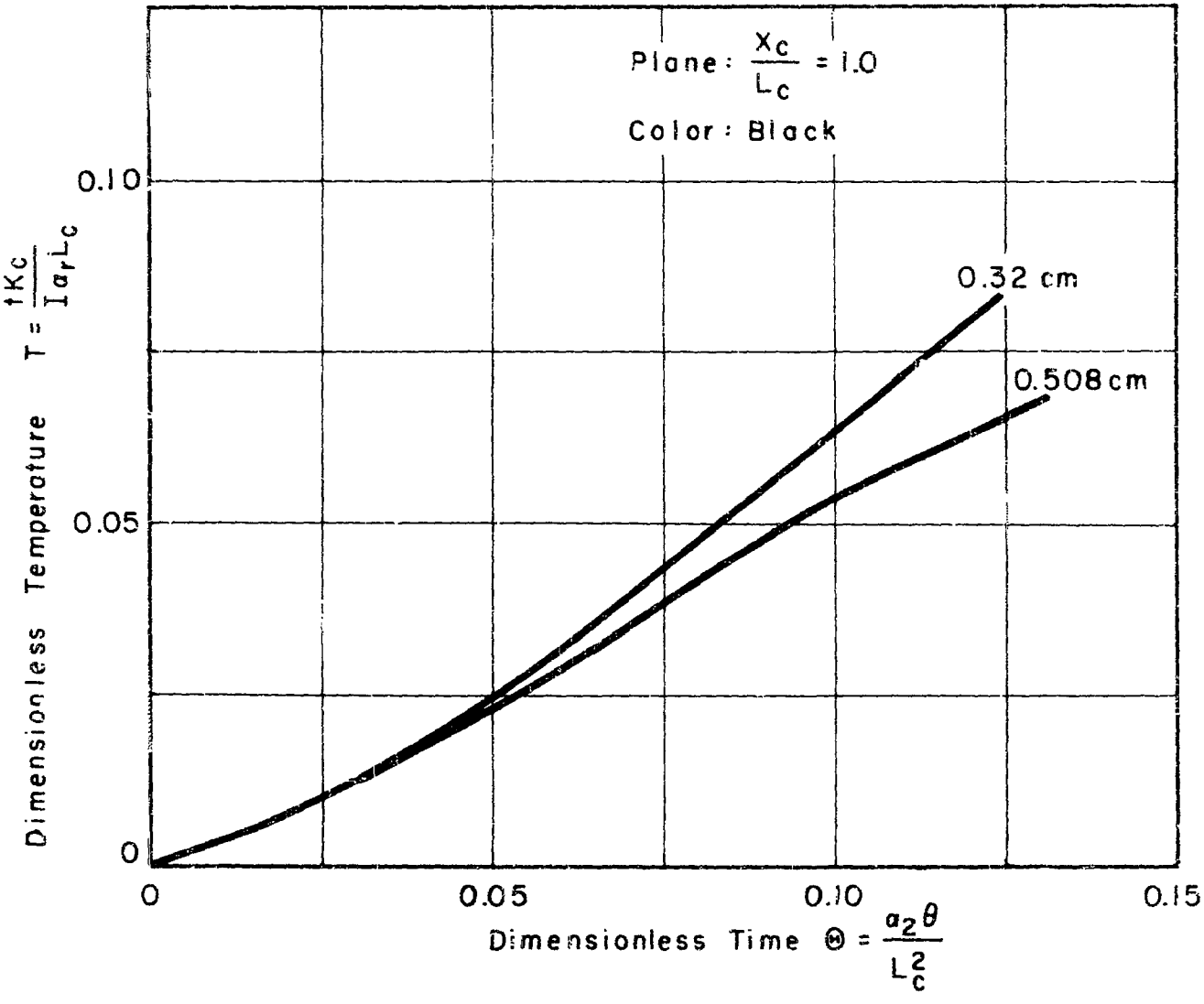

FIG. 7 SPACING EFFECTS

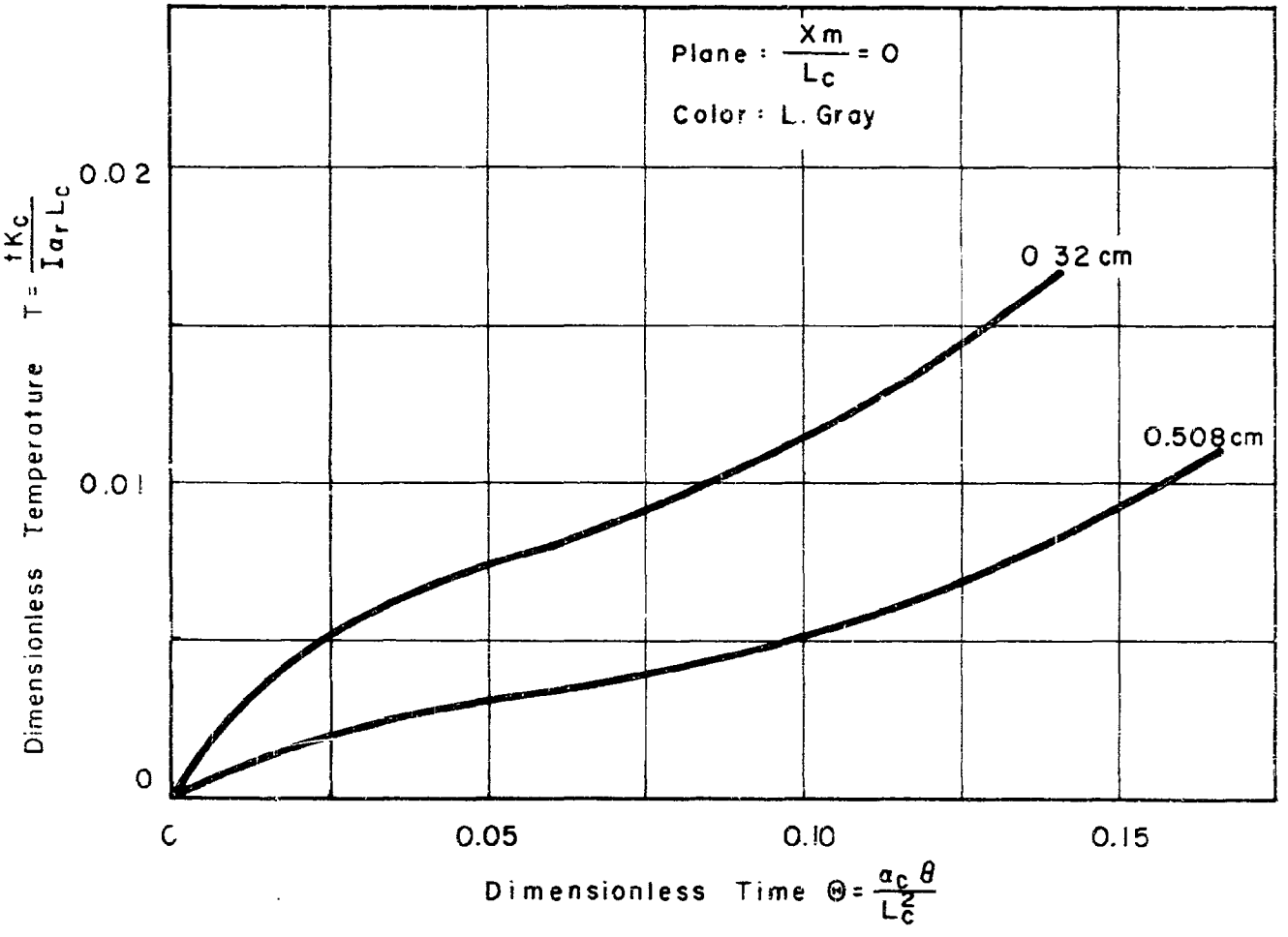

FIG. 8 SPACING EFFECTS

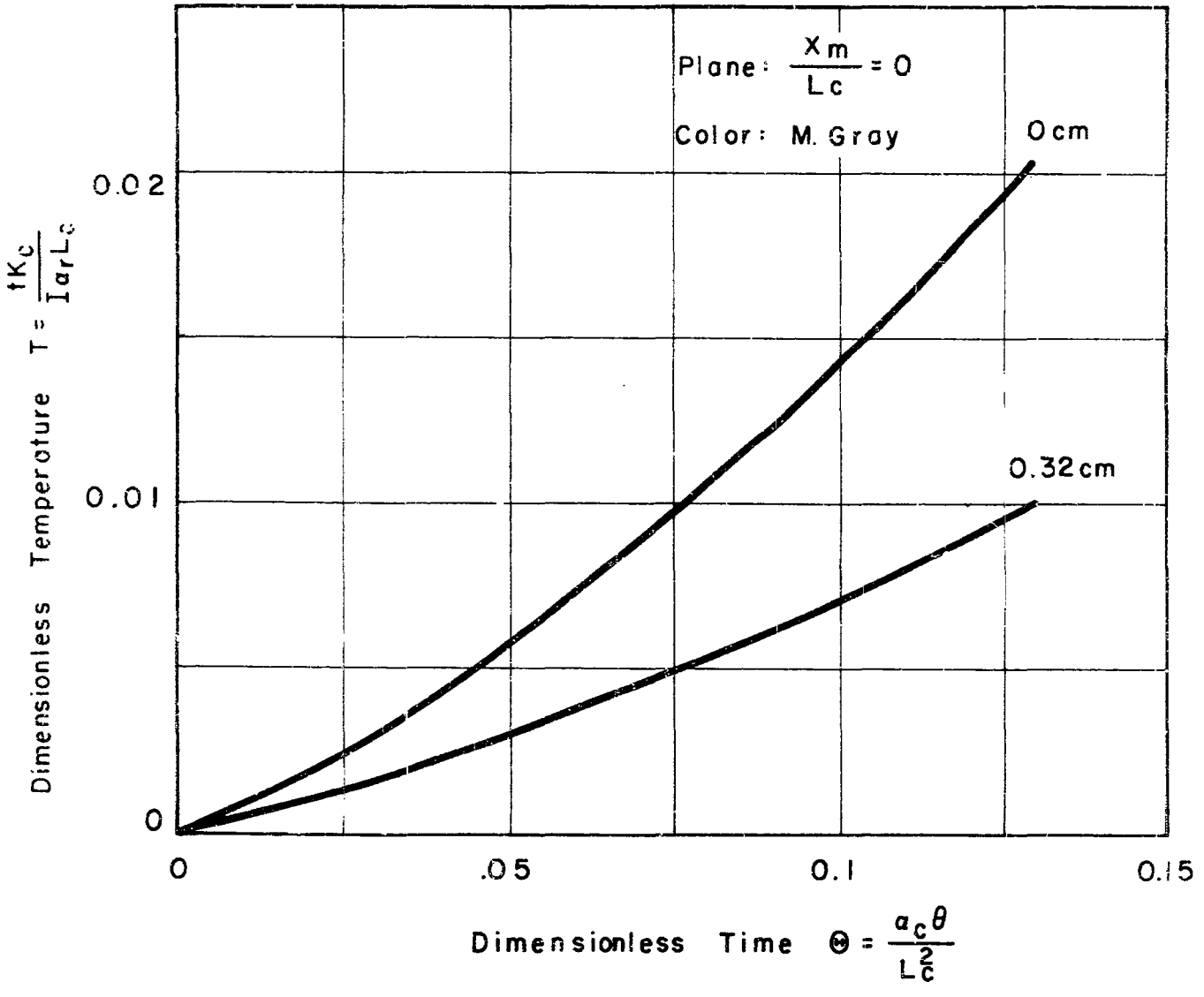

FIG. 9 SPACING EFFECTS

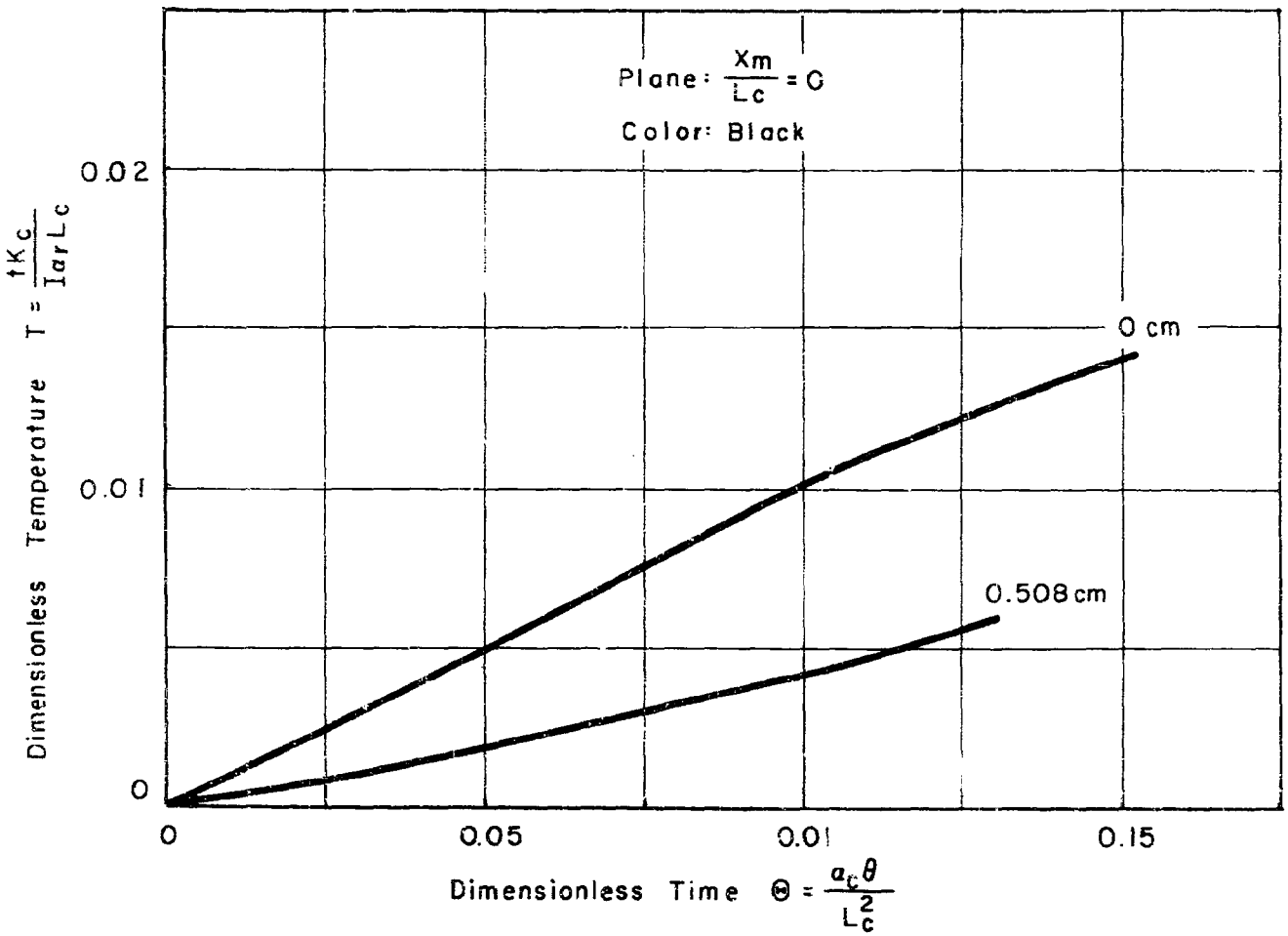

FIG. 10 SPACING EFFECTS

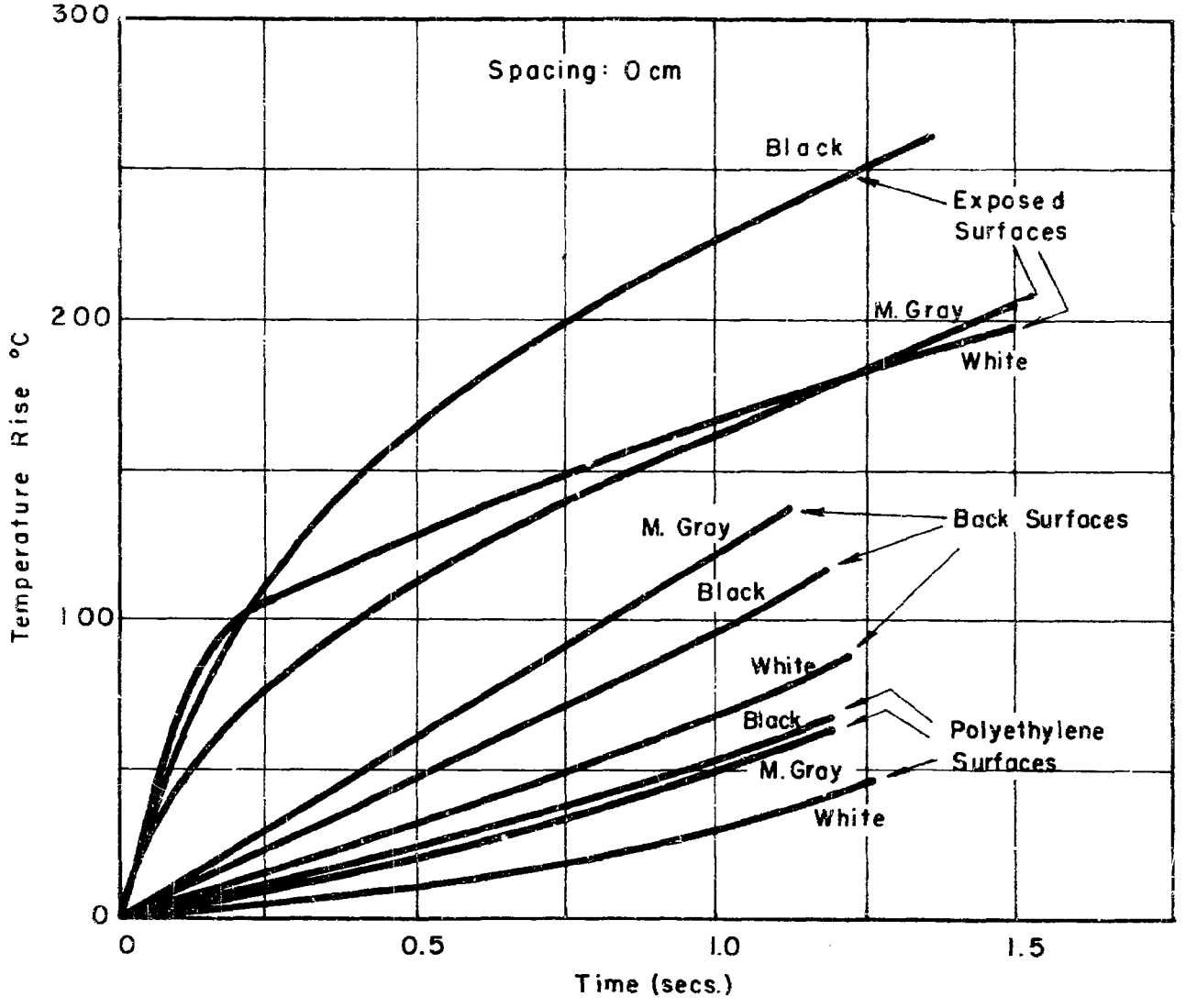

FIG. II COLOR COMPARISON

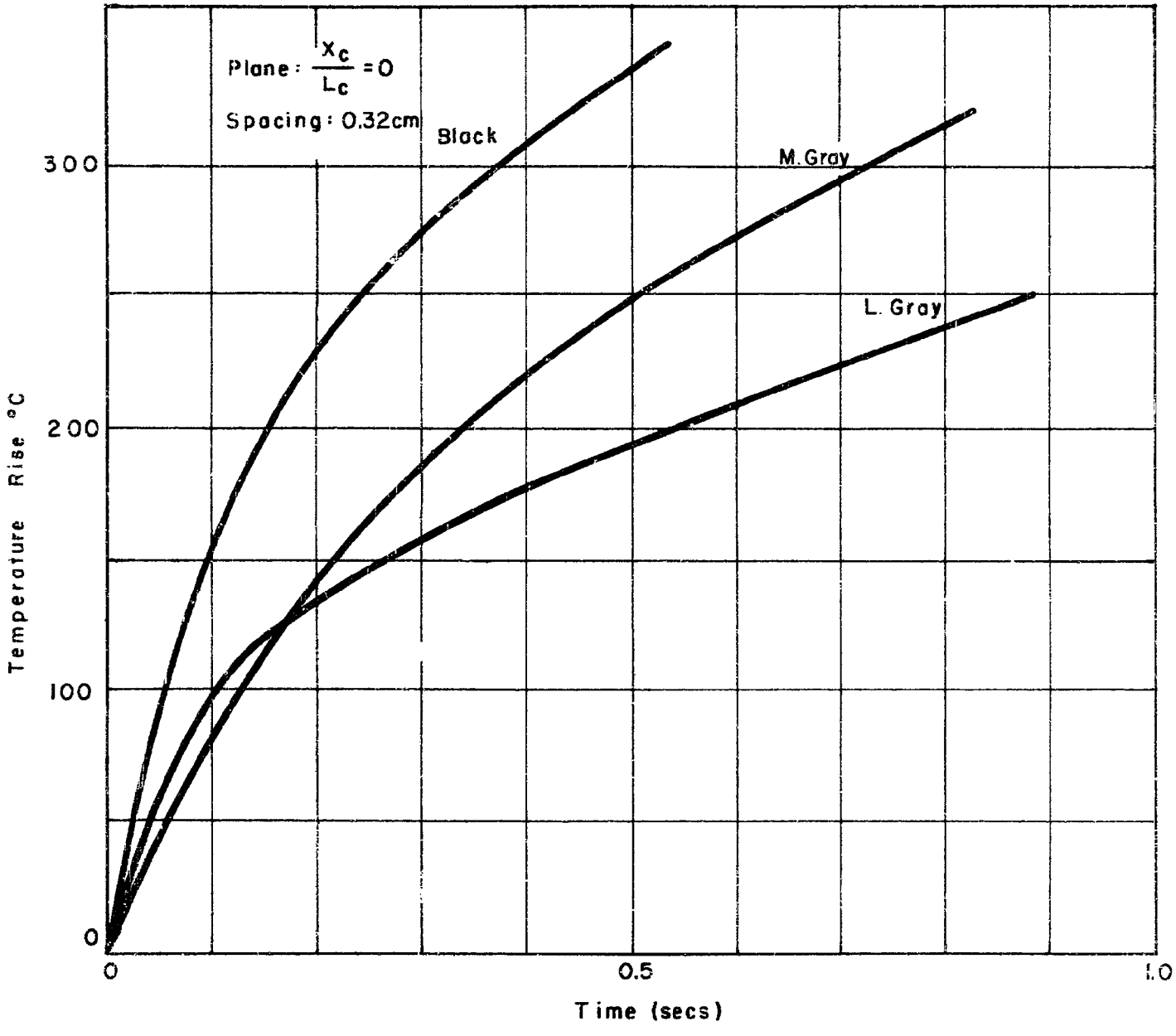

FIG. 12 COLOR COMPARISON

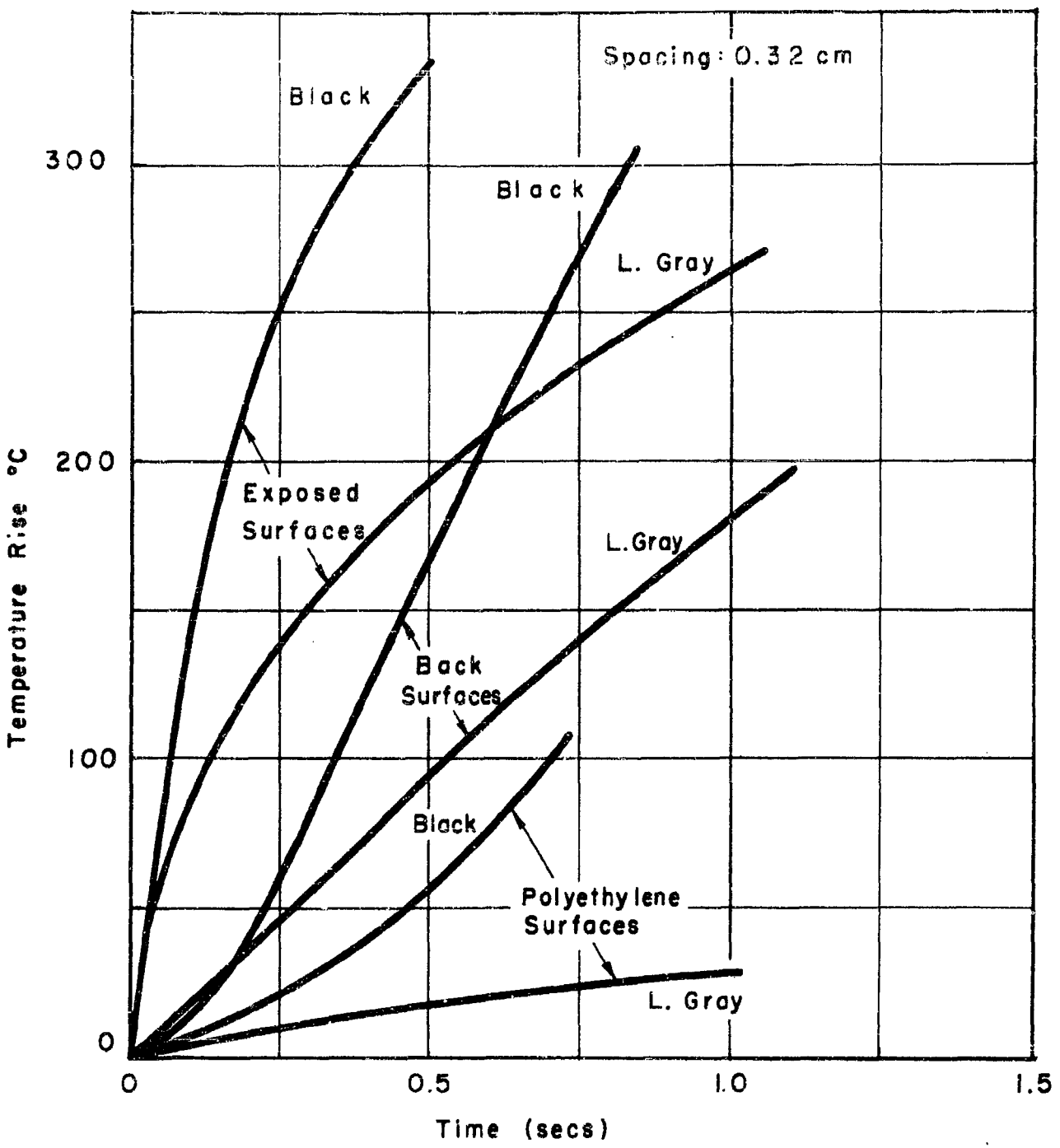

FIG. 13 COLOR COMPARISON

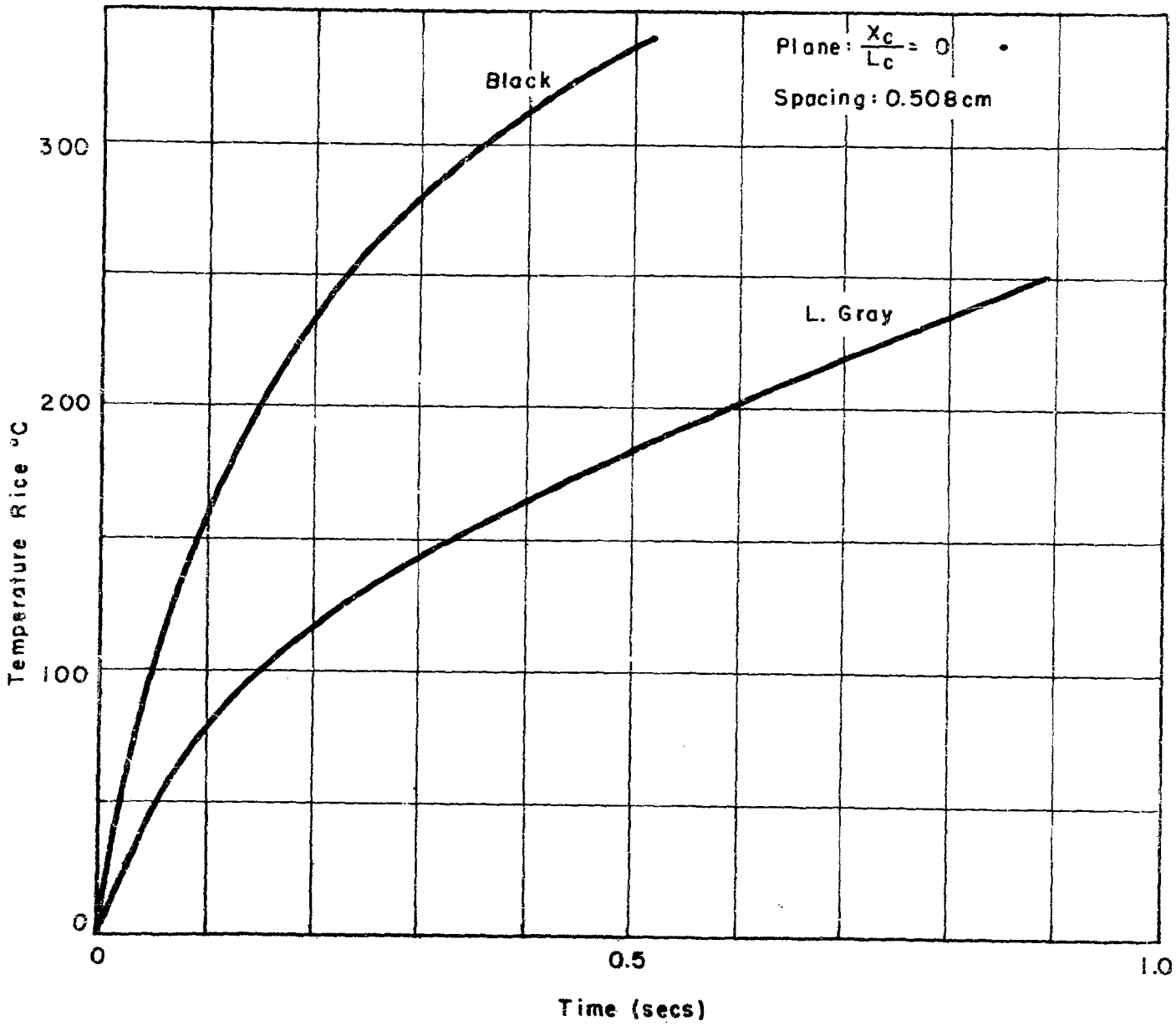

FIG. 14 COLOR COMPARISON

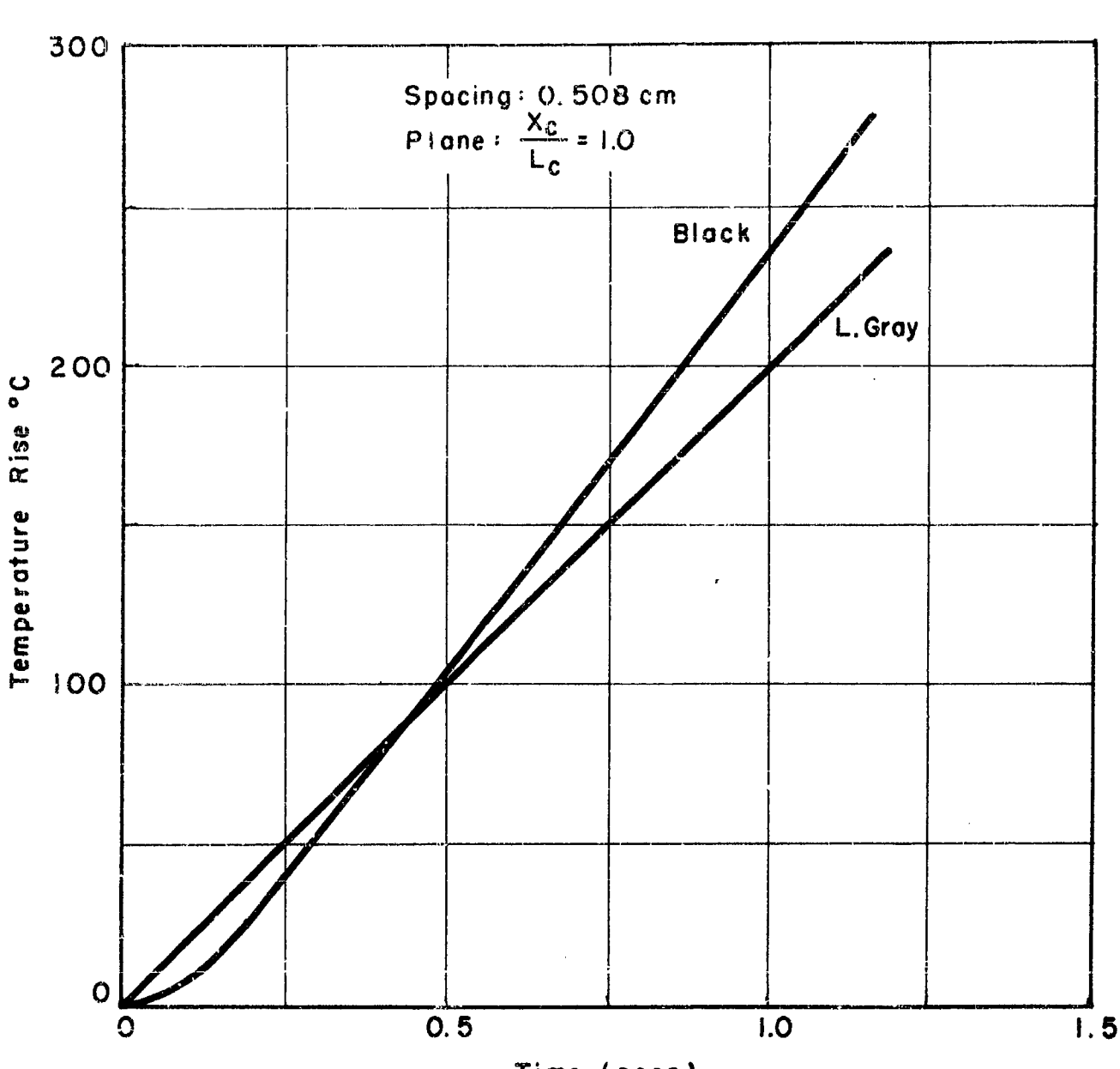

FIG. 15 COLOR COMPARISON

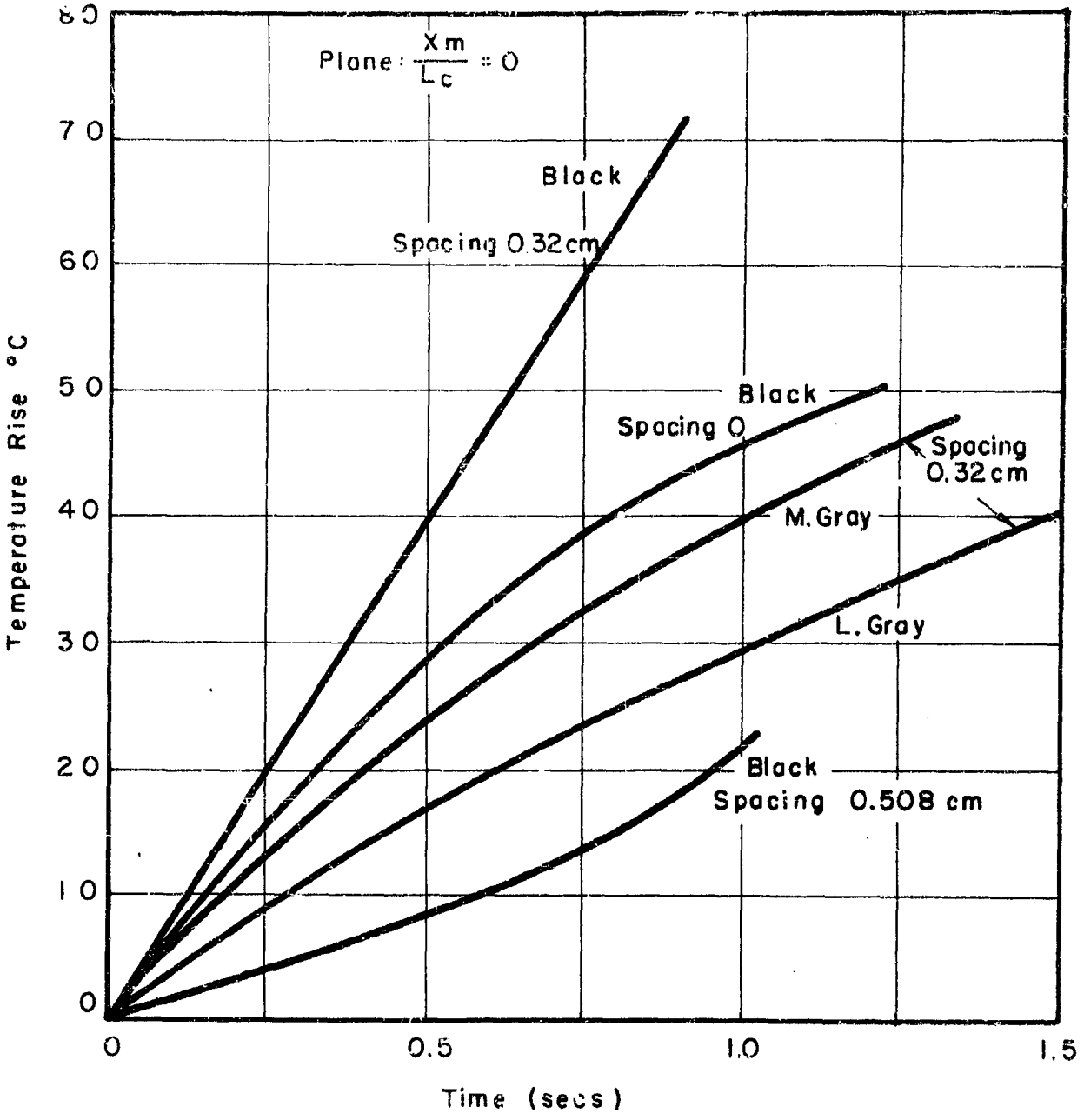

FIG. 16 COLOR COMPARISON & SPACING EFFECTS

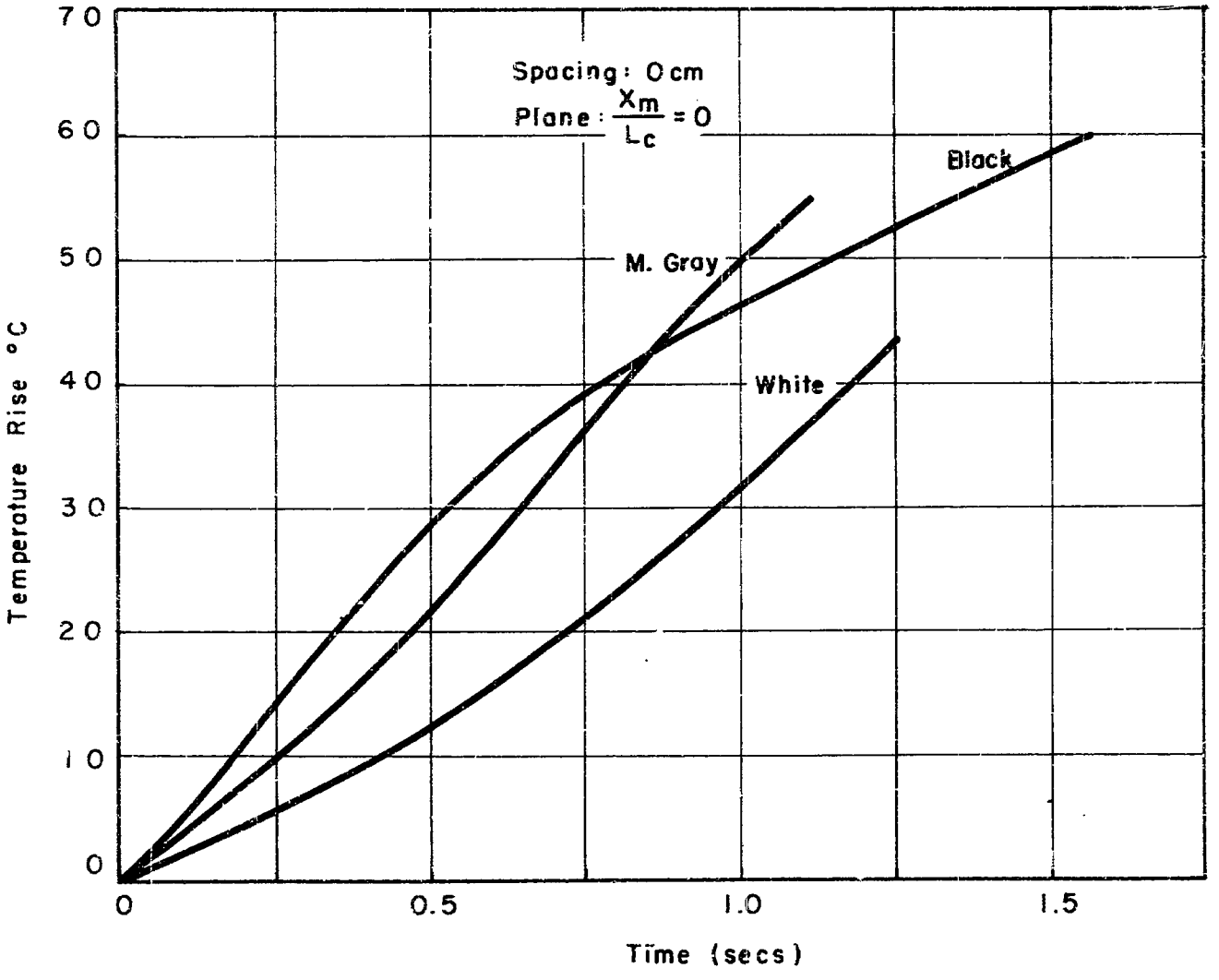

FIG. 17 COLOR COMPARISON

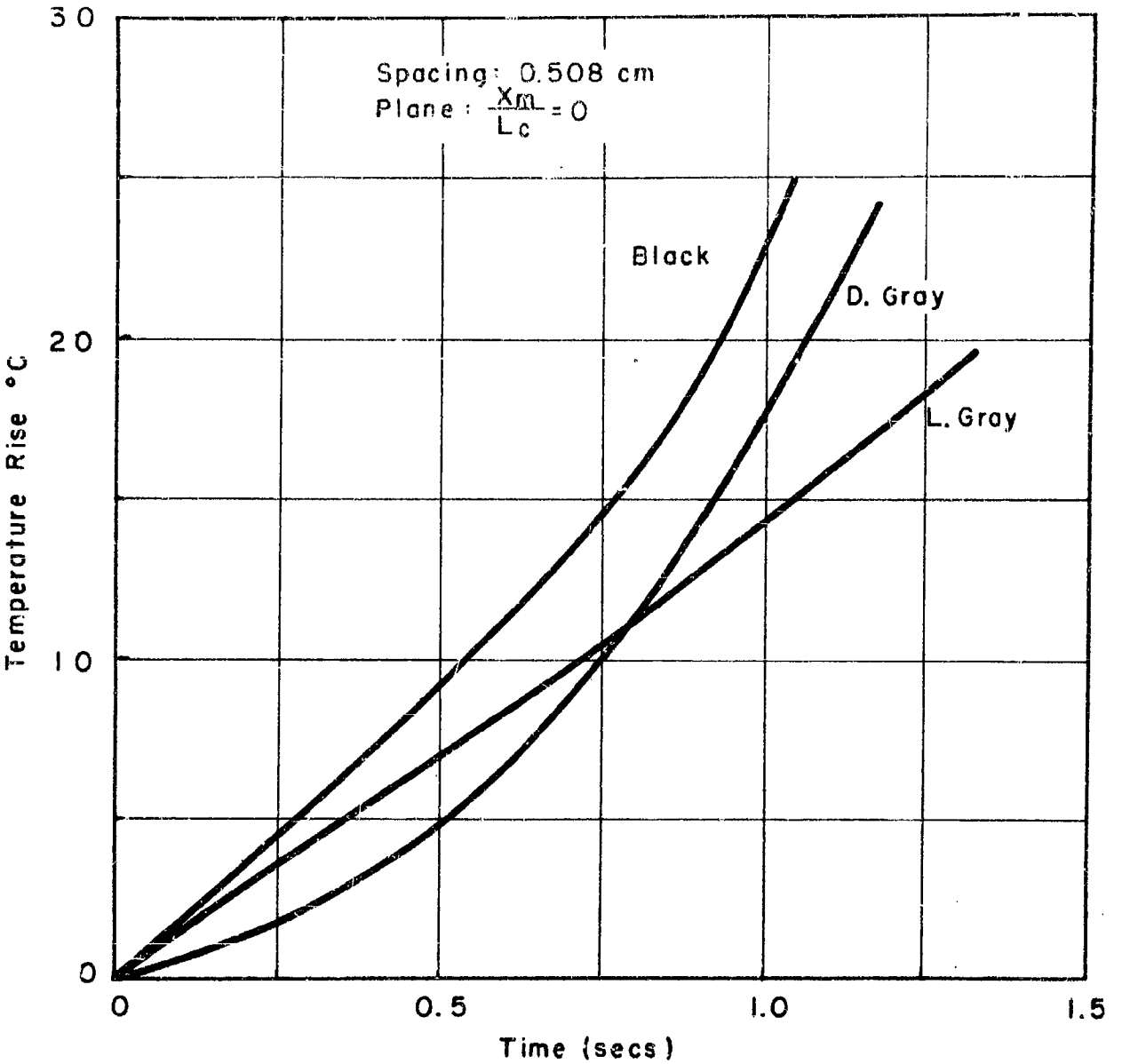

FIG. 18 COLOR COMPARISON

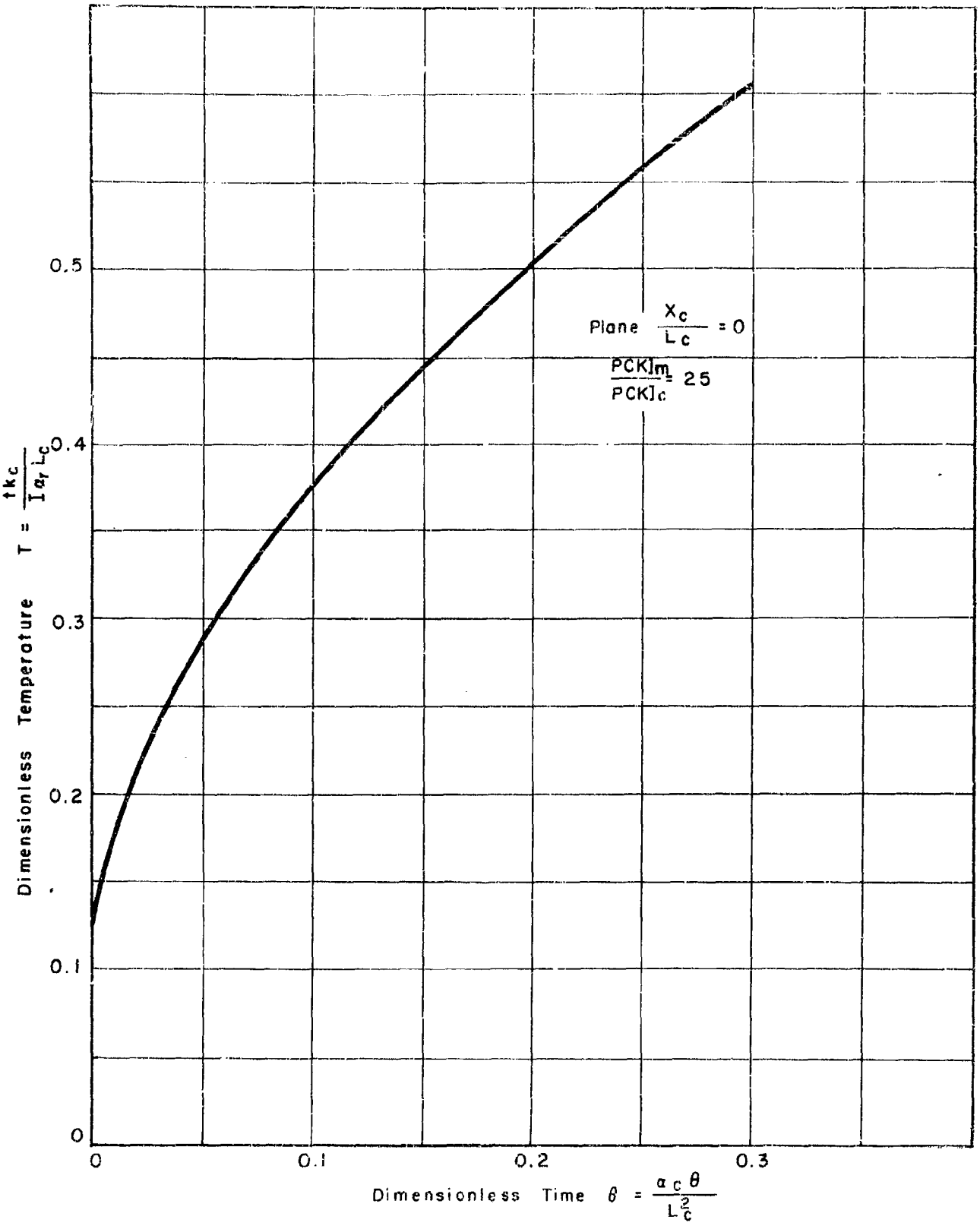

FIG. 19 TEMPERATURE—TIME RELATIONS OF TWO-LAYER SYSTEM FOR $\frac{U_o L_c}{K_c} = 0.1 - 0.2$

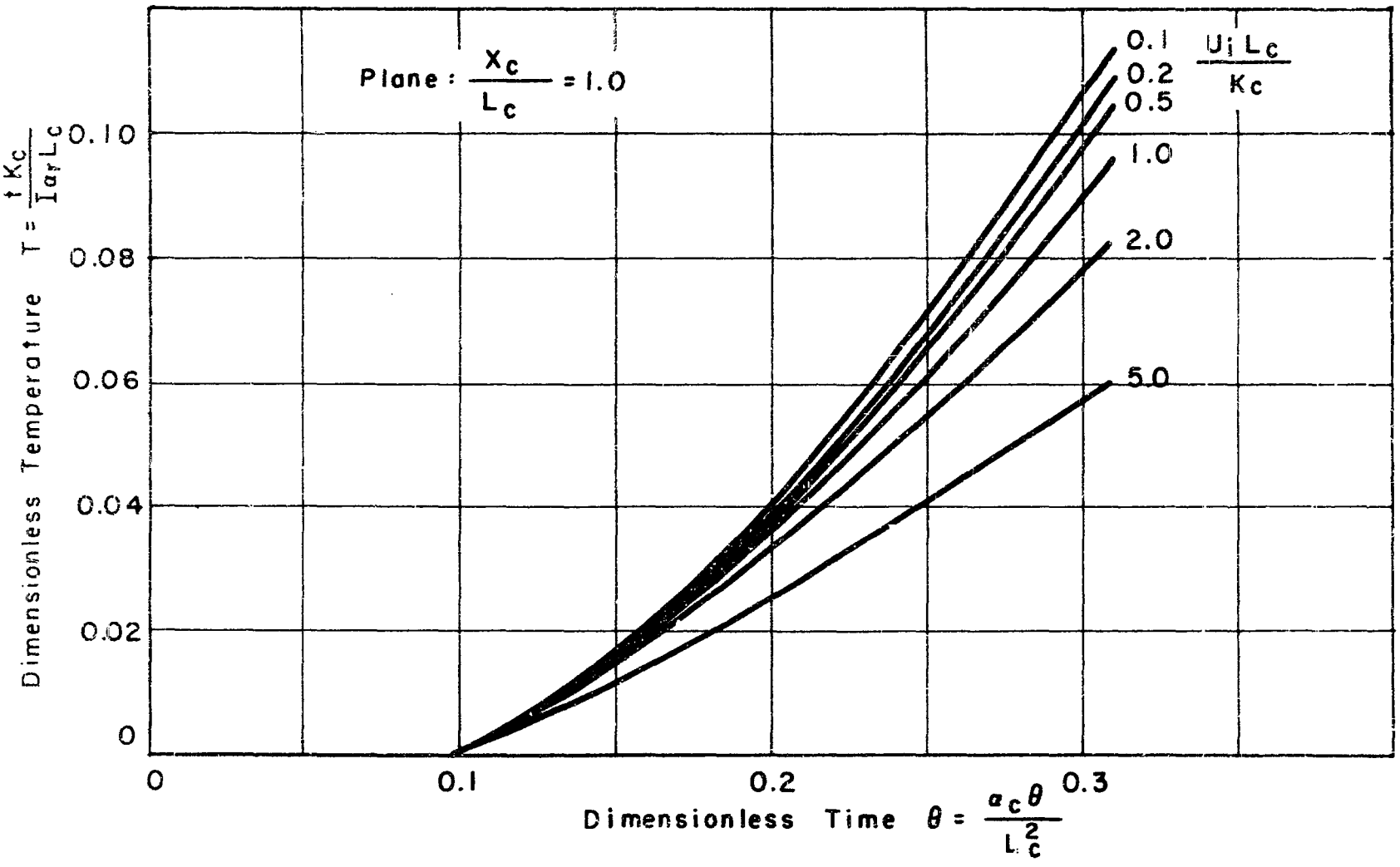

FIG 20 TEMPERATURE - TIME RELATIONS OF TWO-LAYER SYSTEM FOR $\frac{U_o L_c}{K_c} = 0.1$

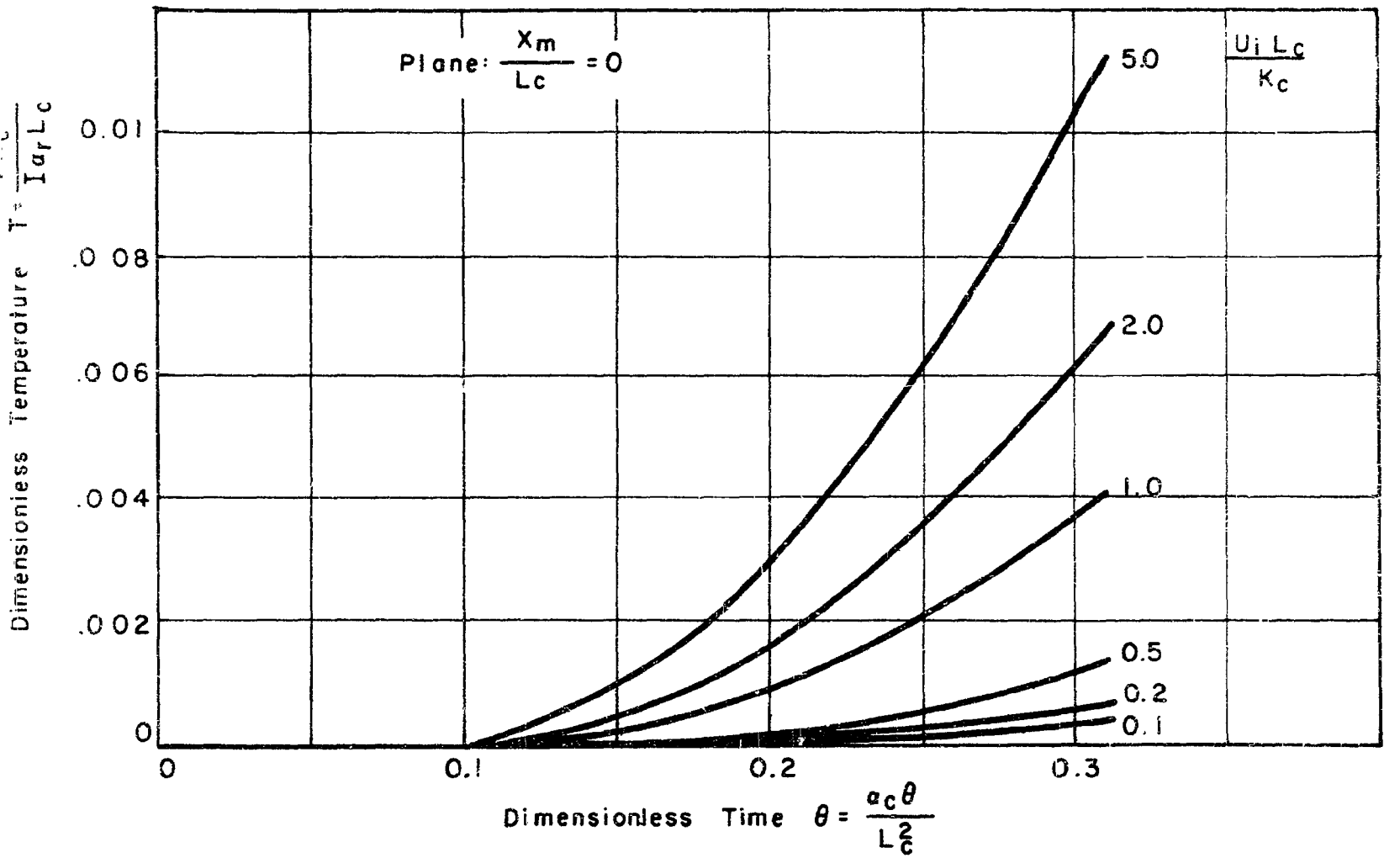

FIG. 21 TEMPERATURE – TIME RELATIONS OF TWO – LAYER SYSTEM FOR $\frac{U_0 L_c}{K_c} = 0.1$

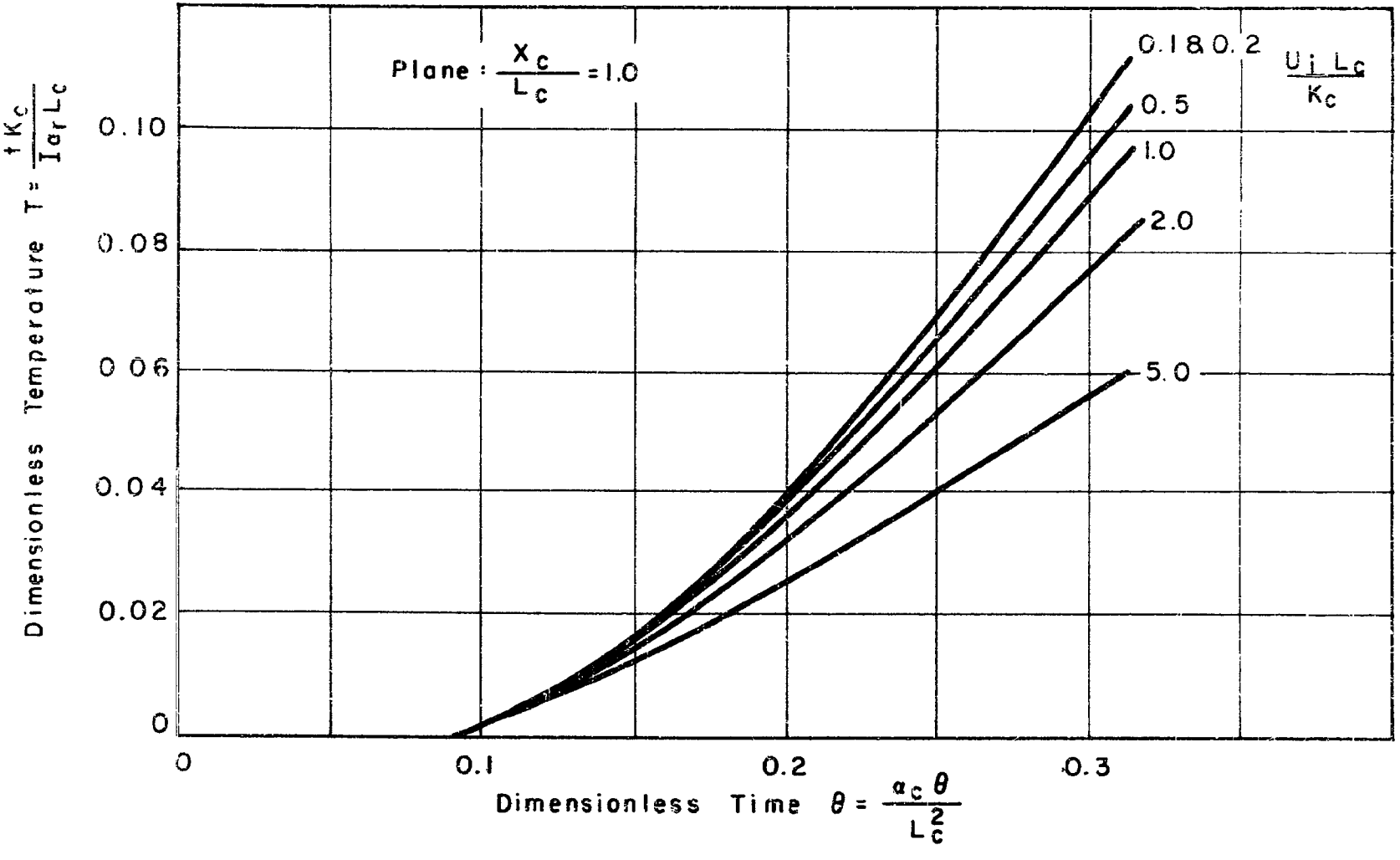

FIG. 22 TEMPERATURE — TIME RELATIONS OF TWO-LAYER SYSTEM FOR $\frac{U_o L_c}{K_c} = 0.15$

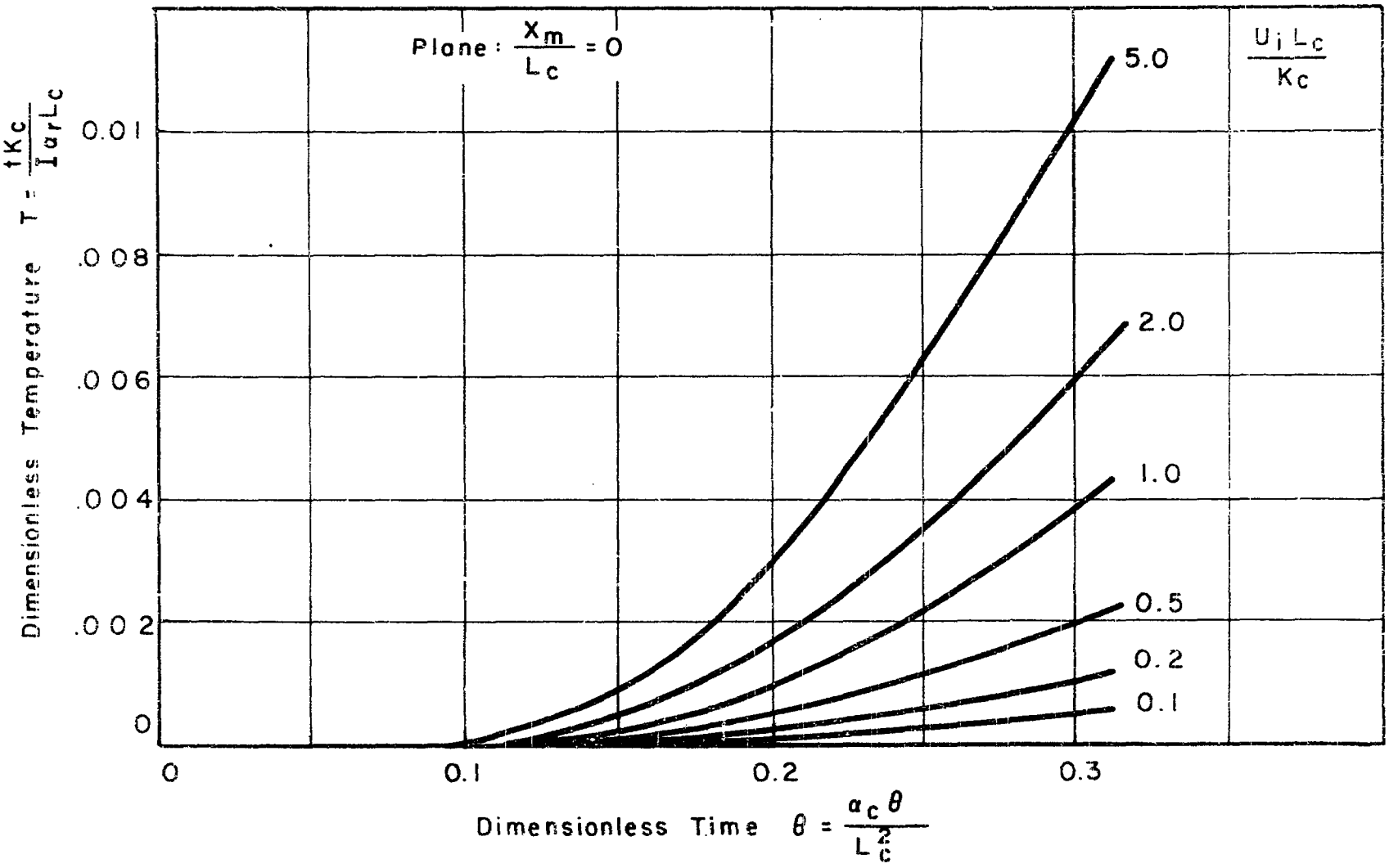

FIG 23 TEMPERATURE — TIME RELATIONS OF TWO-LAYER SYSTEM FOR $\frac{U_o L_c}{K_c} = 0.15$

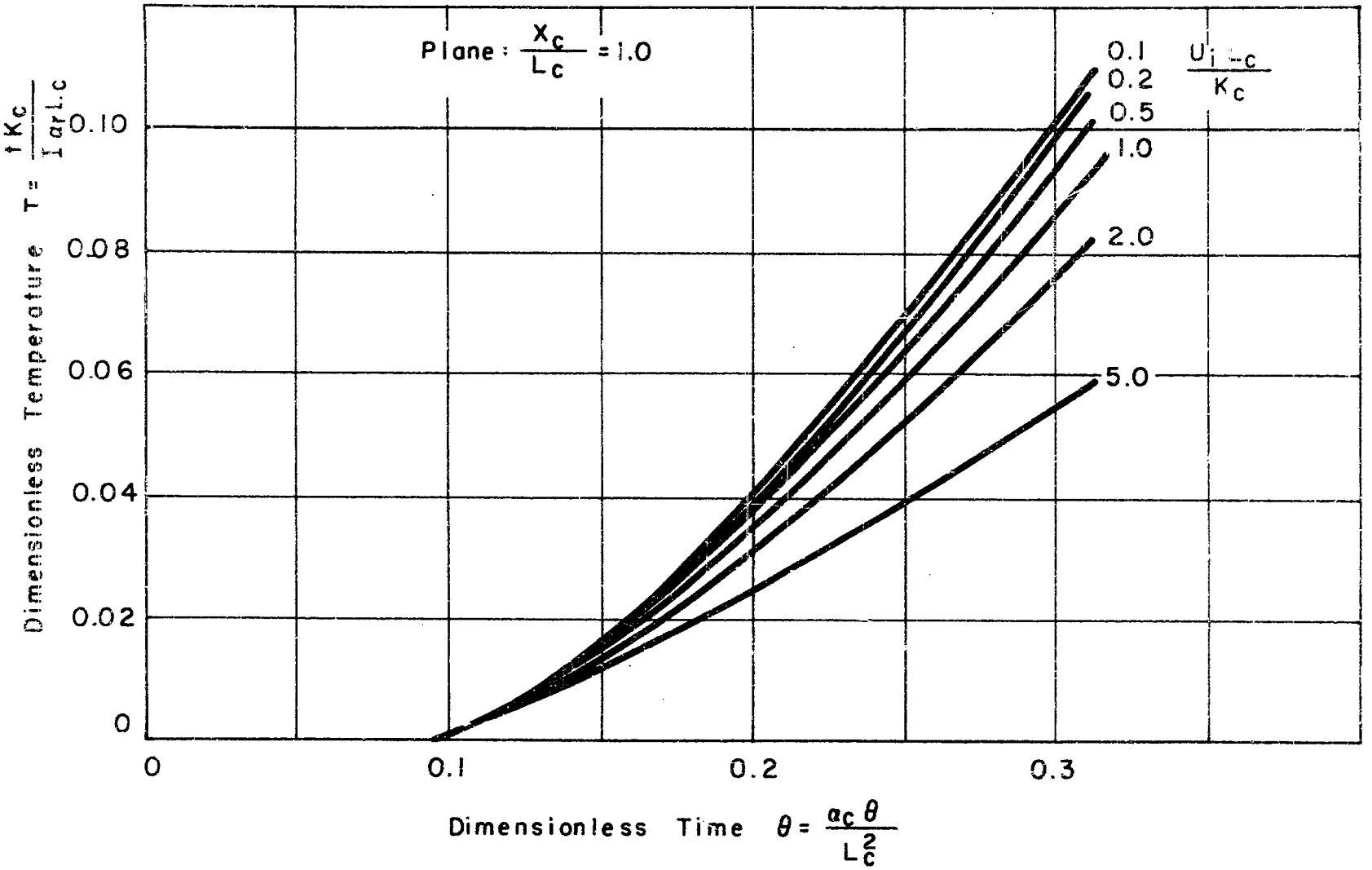

FIG. 24 TEMPERATURE — TIME RELATIONS OF TWO-LAYER SYSTEM FOR $\frac{U_0 L_c}{K_c} = 0.20$

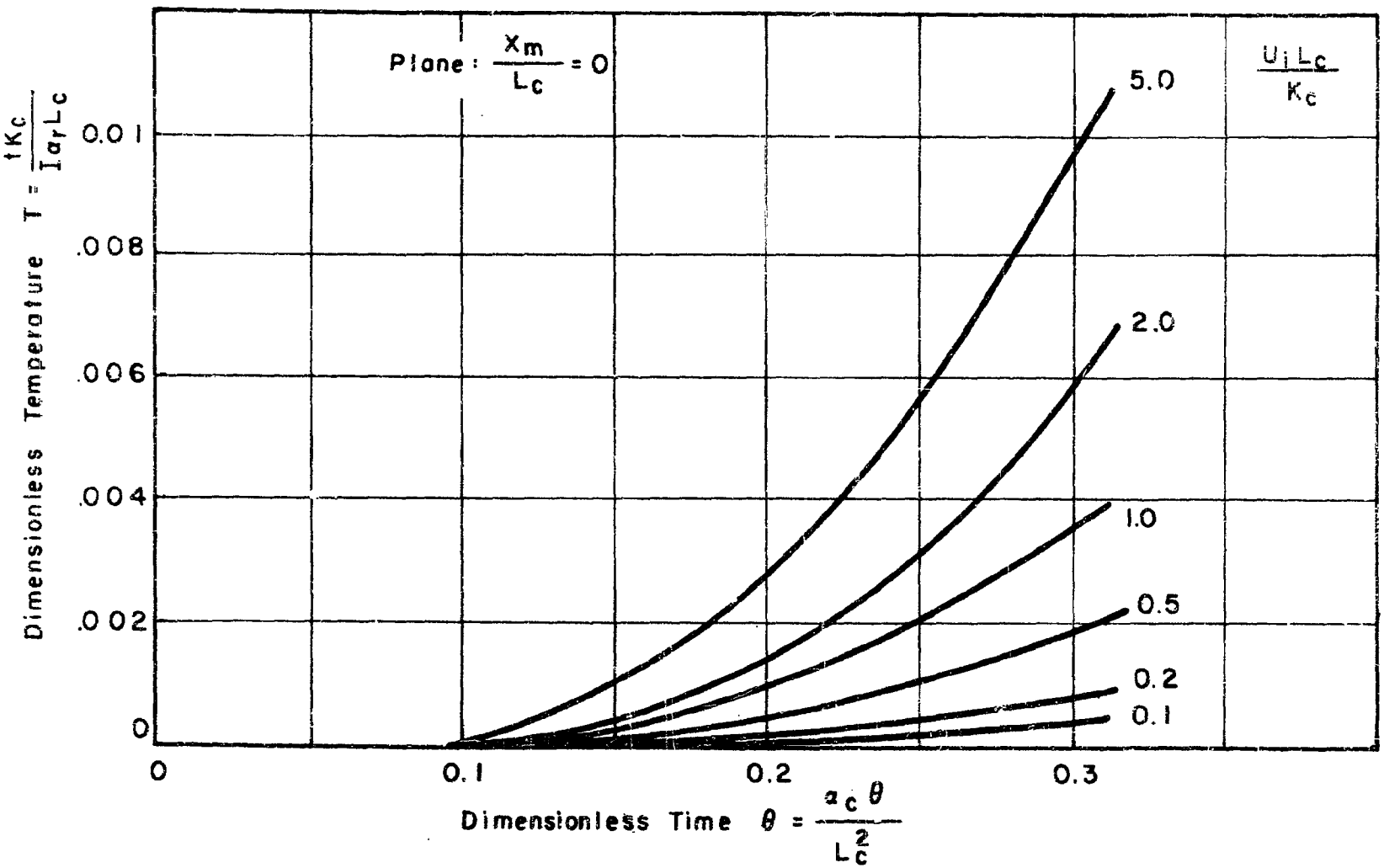

FIG 25 TEMPERATURE – TIME RELATIONS OF TWO-LAYER SYSTEM FOR $\frac{U_0 L_c}{K_c} = 0.20$

FIG. 26

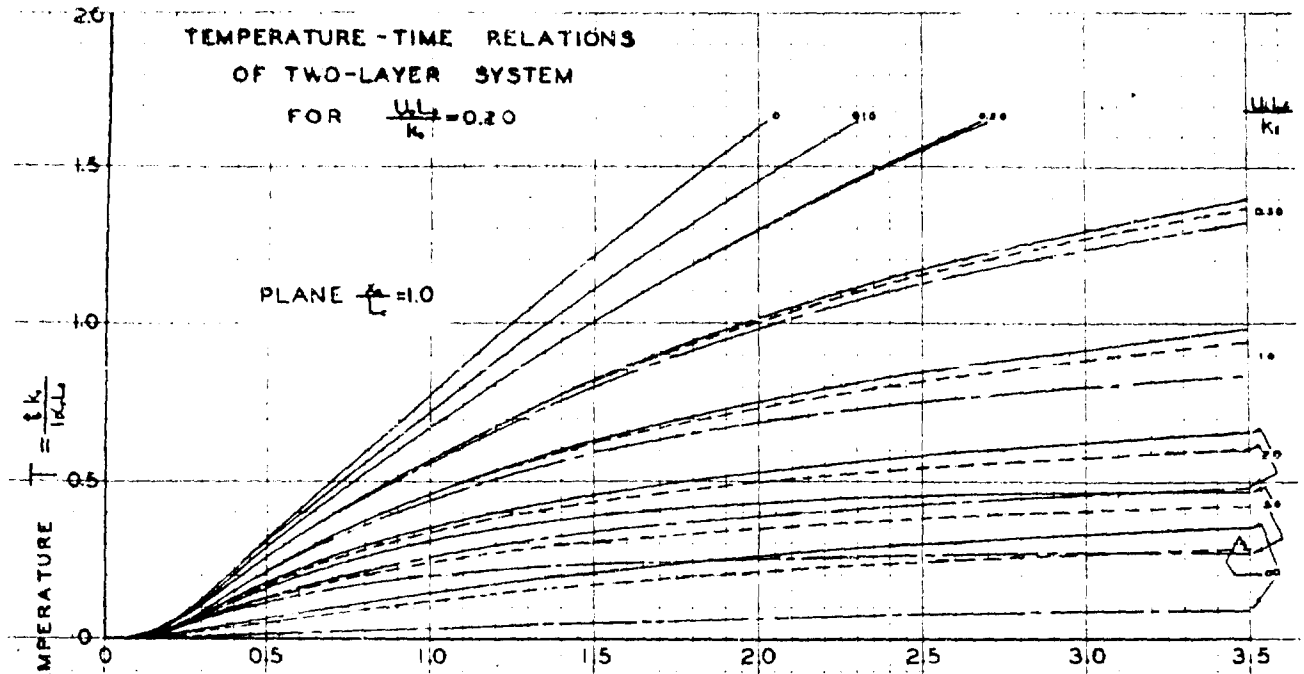
TEMPERATURE - TIME RELATIONS
OF TWO-LAYER SYSTEM
FOR $\frac{U_1 L_2}{K_2} = 0.20$
PLANE $\frac{x_1}{L_1} = 1.0$
$T = \frac{t\, k_2}{U_1 L_2}$
DIMENSIONLESS TEMPERATURE
$\frac{U_1 L_1}{K_1}$
0
0.10
0.20
0.30
1.0
2.0
3.0
5.0
∞
0
0.5
1.0
1.5
2.0
2.5
3.0
3.5

FIG. 27

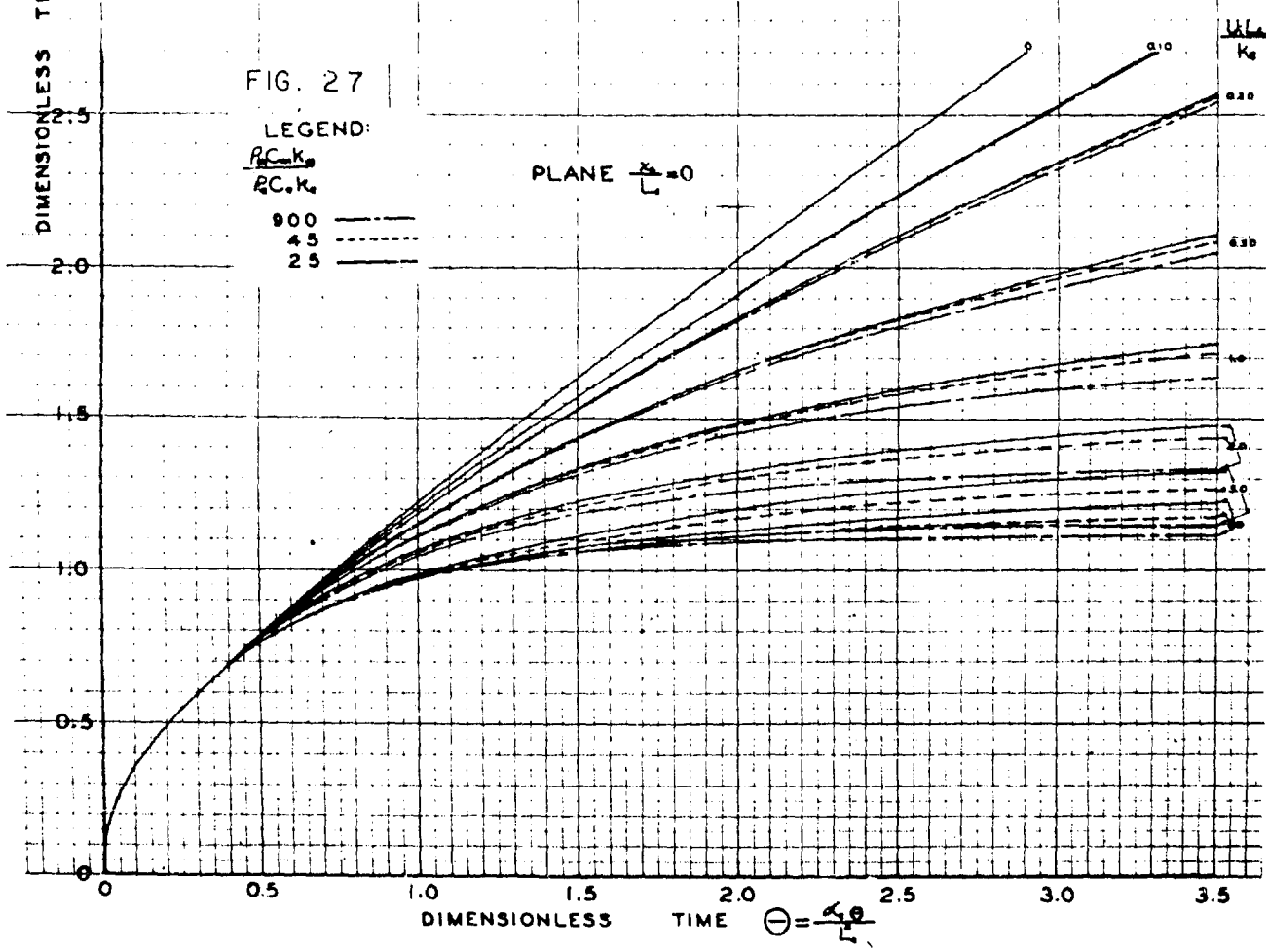
LEGEND:
$\frac{\rho_1 C_1 k_1}{\rho_2 C_2 k_2}$
900
45
25
PLANE $\frac{x_1}{L_1} = 0$
$\frac{U_2 L_2}{K_2}$
0
0.10
0.20
0.30
1.0
2.0
3.0
5.0
∞
DIMENSIONLESS TEMPERATURE
DIMENSIONLESS TIME $\Theta = \frac{\alpha_2 \theta}{L_2^2}$
0
0.5
1.0
1.5
2.0
2.5
3.0
3.5

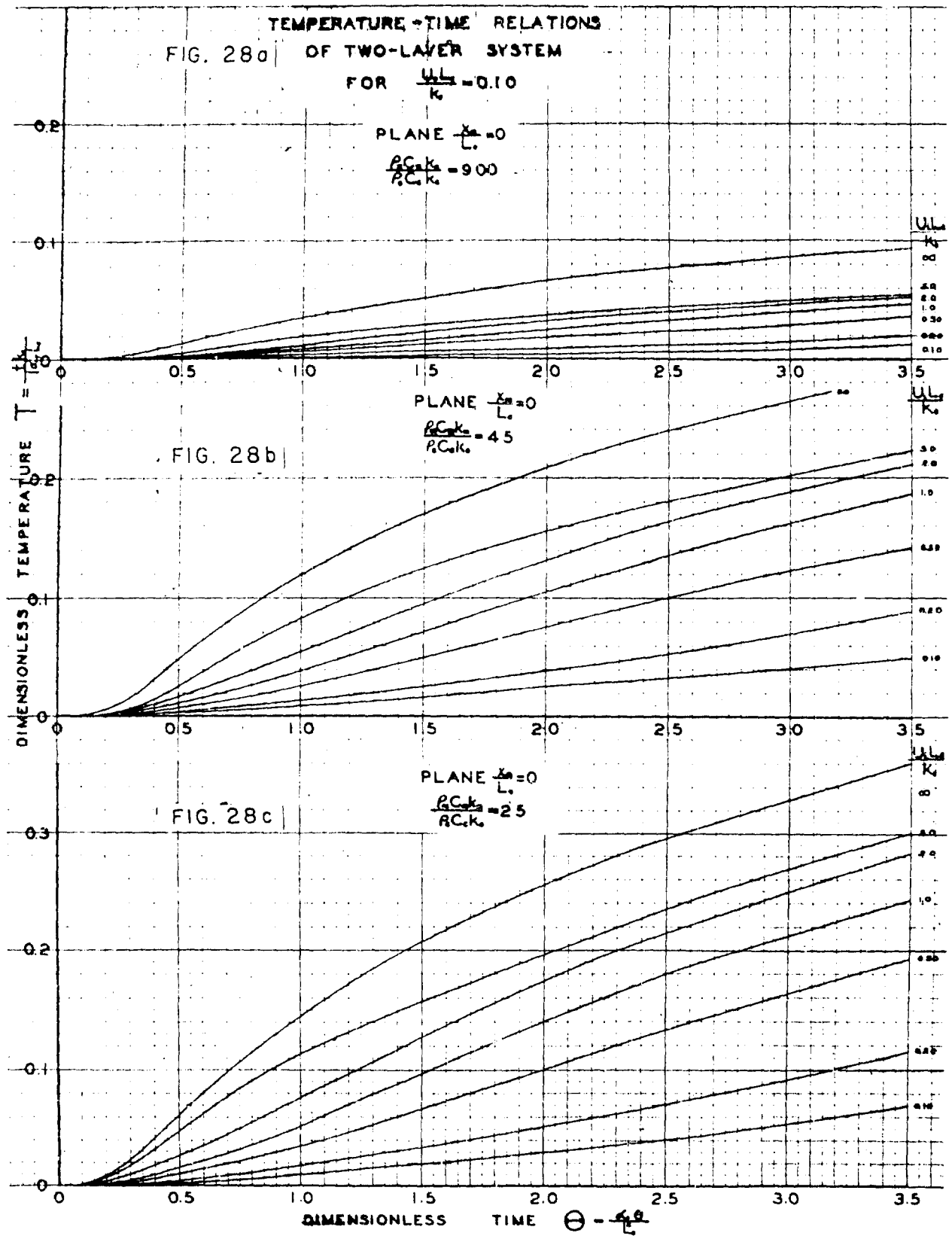
TEMPERATURE - TIME RELATIONS
OF TWO-LAYER SYSTEM
FOR $\frac{U_1 L_1}{k_1} = 0.10$
FIG. 28a
PLANE $\frac{x_m}{L_1} = 0$
$\frac{\rho_2 C_2 k_2}{\rho_1 C_1 k_1} = 900$
FIG. 28b
PLANE $\frac{x_m}{L_1} = 0$
$\frac{\rho_2 C_2 k_2}{\rho_1 C_1 k_1} = 45$
FIG. 28c
PLANE $\frac{x_m}{L_1} = 0$
$\frac{\rho_2 C_2 k_2}{\rho_1 C_1 k_1} = 2.5$
DIMENSIONLESS TEMPERATURE $T = \frac{t k_1}{U_1 L_1^2}$
DIMENSIONLESS TIME $\Theta = \frac{k_1 \theta}{L_1^2}$
0
0.5
1.0
1.5
2.0
2.5
3.0
3.5
0.1
0.2
0.3

FIG. 29

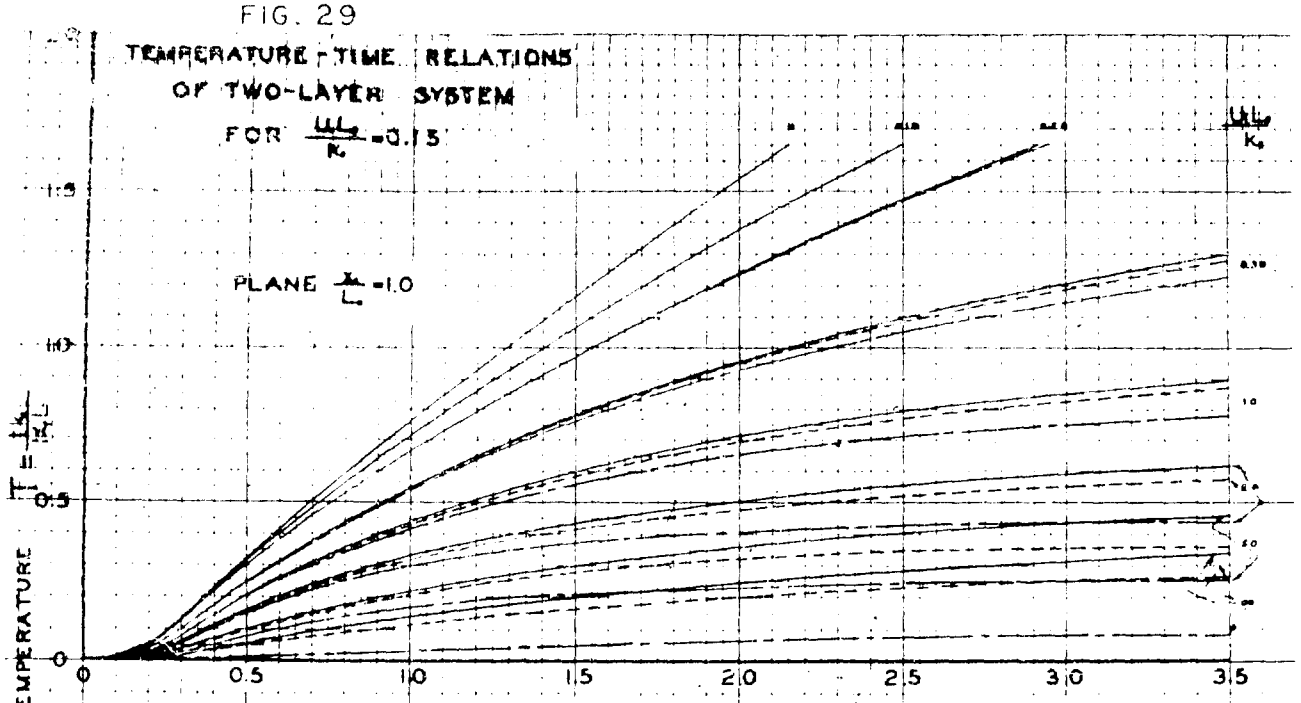
TEMPERATURE - TIME RELATIONS
OF TWO-LAYER SYSTEM
FOR $\frac{U_1 L_2}{K_2} = 0.15$
PLANE $\frac{x_1}{L_1} = 1.0$
$T = \frac{t_1}{t_2 - t_1}$
DIMENSIONLESS TEMPERATURE
0
0.5
1.0
1.5
2.0
2.5
3.0
3.5

FIG. 30

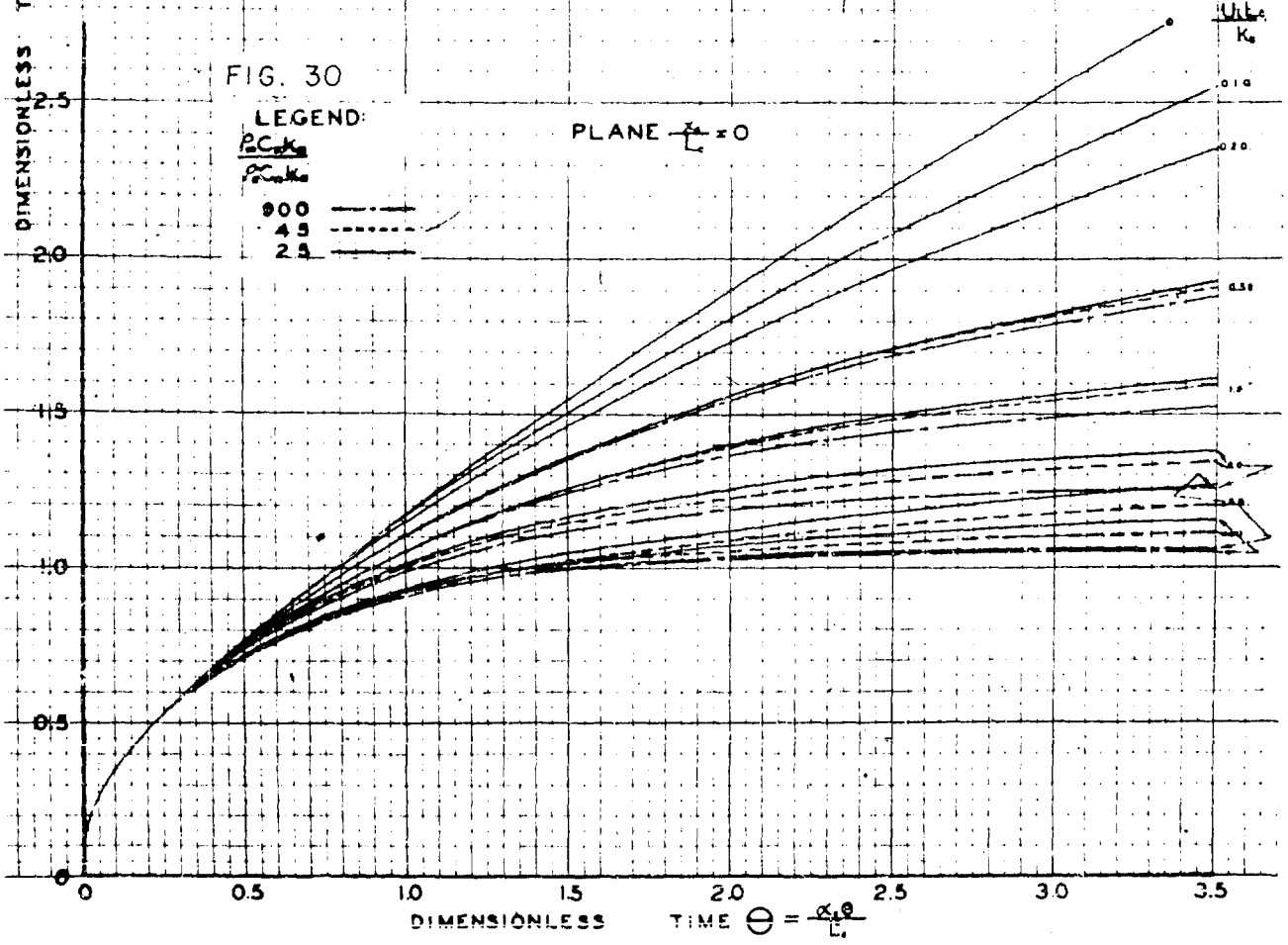
LEGEND:
$\frac{\rho_2 C_2 K_2}{\rho_1 C_1 K_1}$
900
4.9
2.5
PLANE $\frac{x_1}{L_1} = 0$
DIMENSIONLESS TEMPERATURE
DIMENSIONLESS TIME $\Theta = \frac{\alpha_1 \theta}{L_1^2}$
0
0.5
1.0
1.5
2.0
2.5
3.0
3.5

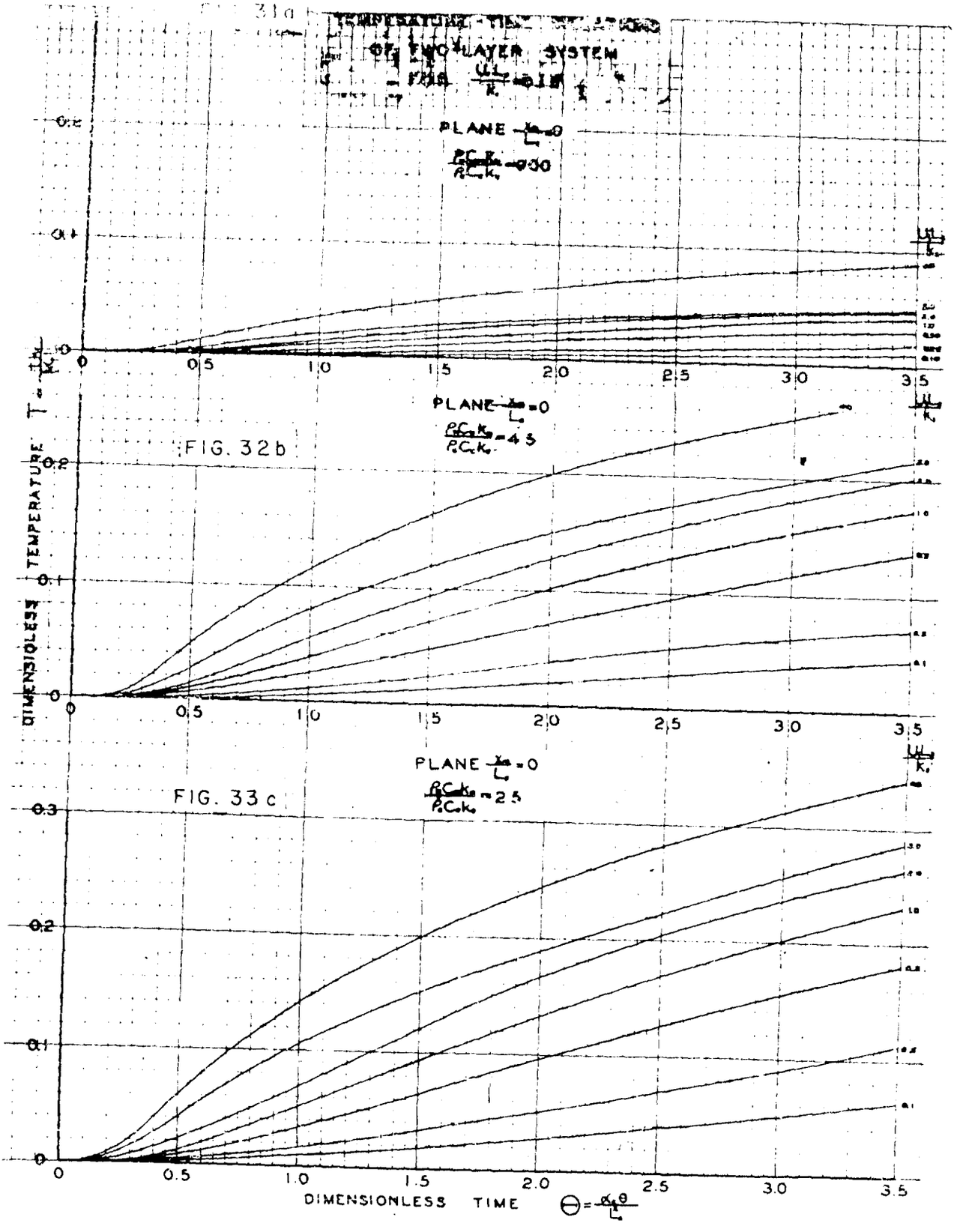

FIG. 32b

FIG. 33c

FIG. 34

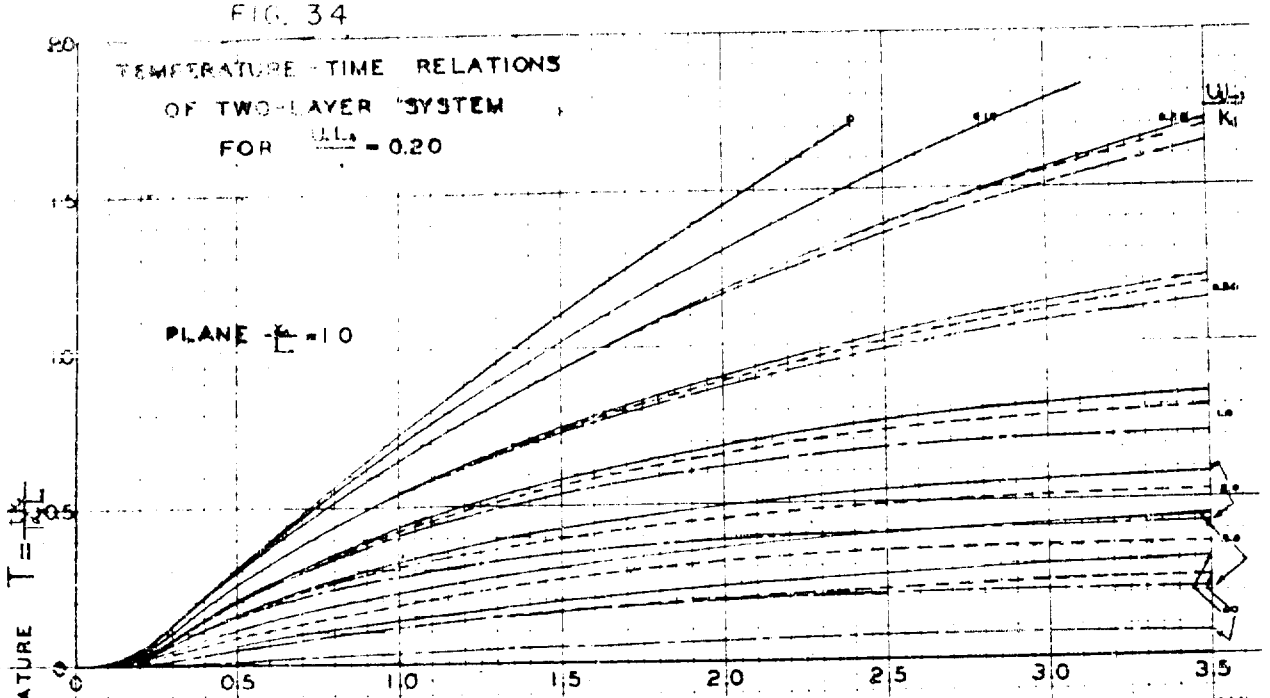
TEMPERATURE - TIME RELATIONS
OF TWO-LAYER SYSTEM
FOR $\frac{L_1}{L_2} = 0.20$
PLANE $\frac{x}{L} = 1.0$
$\frac{U L_2}{K_1}$
DIMENSIONLESS TEMPERATURE $T = \frac{U x}{K_2}$
0.5
1.0
1.5
2.0
2.5
3.0
3.5

FIG. 35

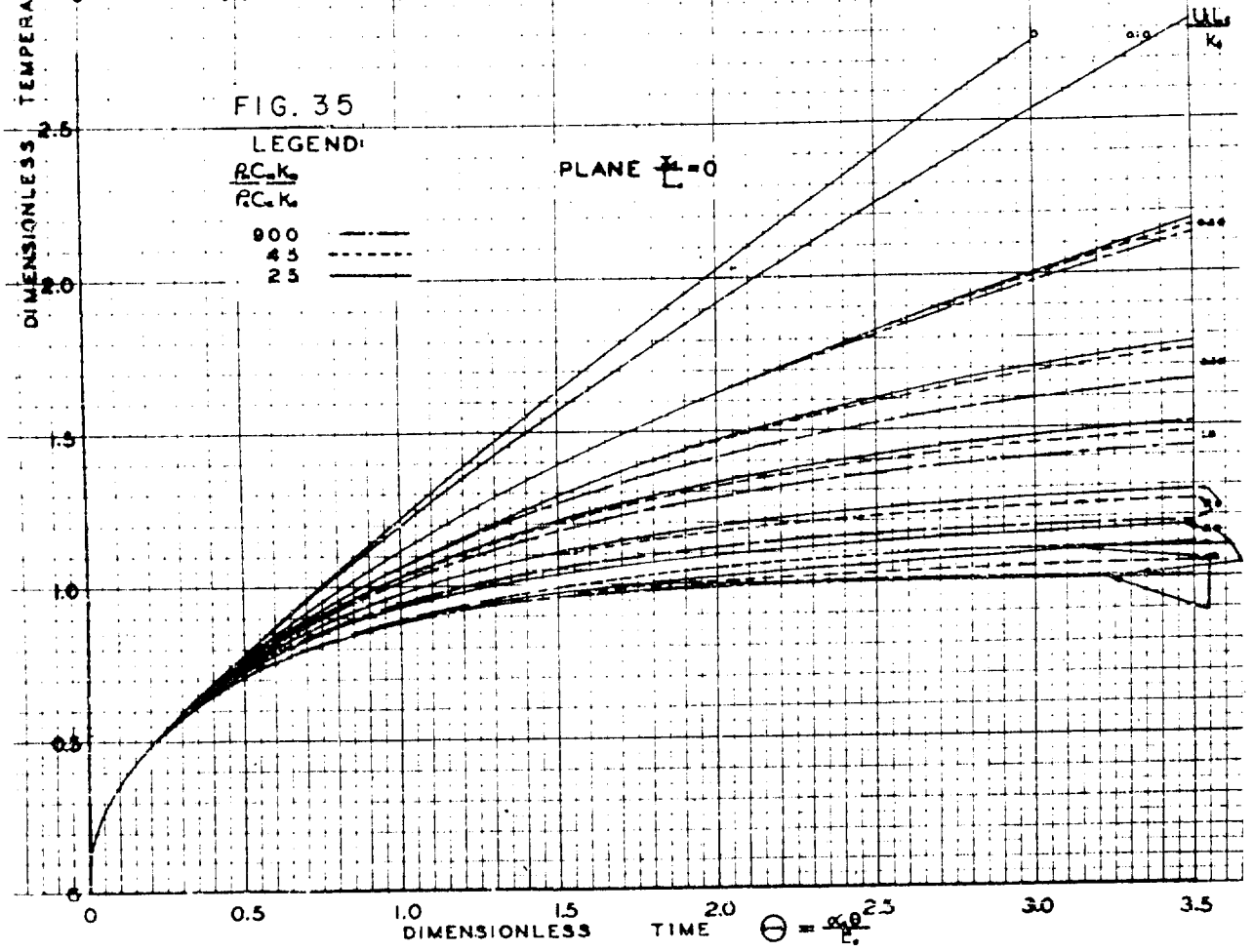
LEGEND
$\frac{\rho C_2 K_2}{\rho C_1 K_1}$
900
45
25
PLANE $\frac{x}{L} = 0$
$\frac{U L_2}{K_2}$
DIMENSIONLESS TEMPERATURE
DIMENSIONLESS TIME $\Theta = \frac{\alpha_2 \theta}{L_2^2}$
0
0.5
1.0
1.5
2.0
2.5
3.0
3.5

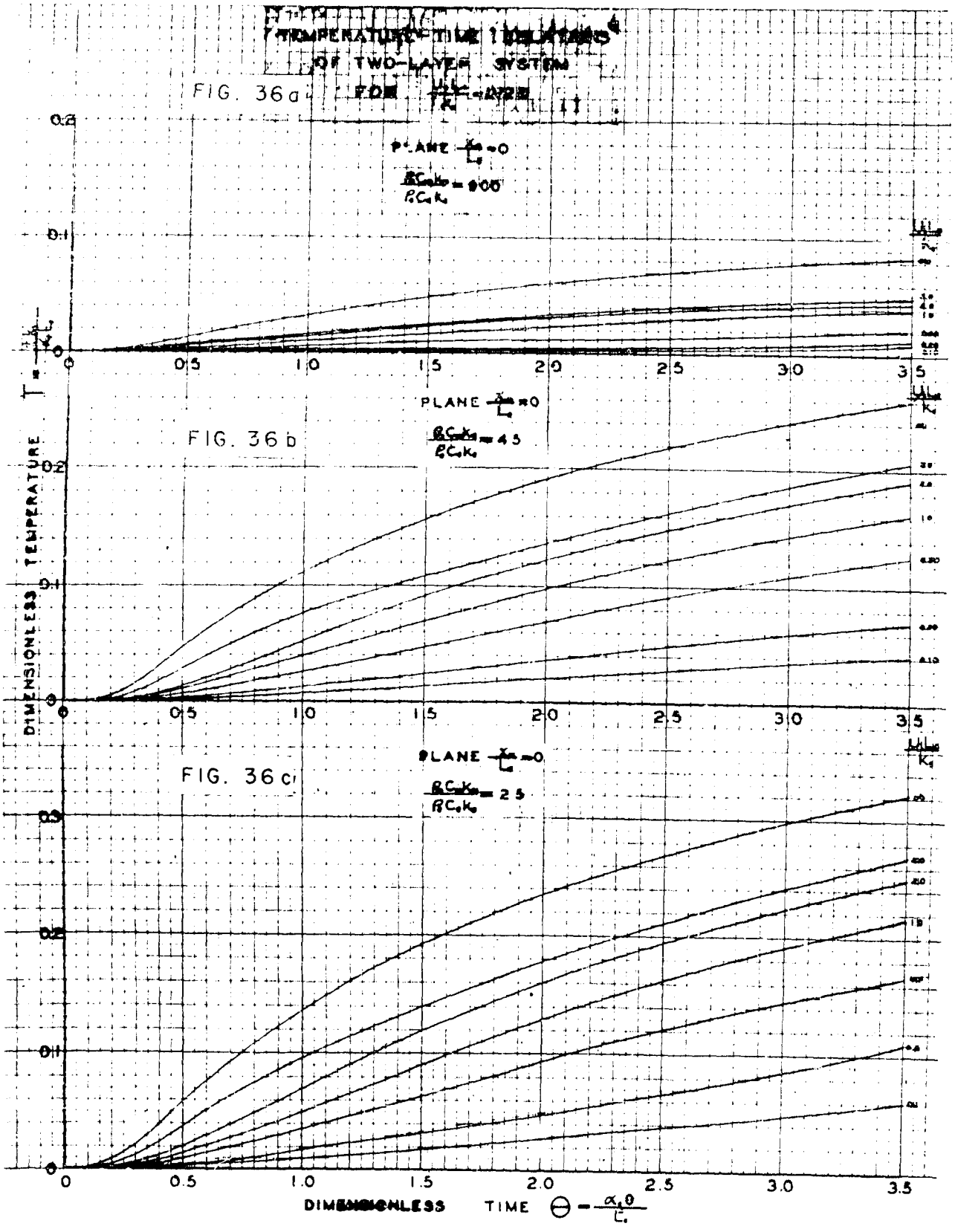
TEMPERATURE-TIME RELATIONS
OF TWO-LAYER SYSTEM
FOR
FIG. 36a
PLANE
FIG. 36b
PLANE
FIG. 36c
PLANE
DIMENSIONLESS TEMPERATURE
DIMENSIONLESS TIME

DISTRIBUTION LIST FOR TECHNICAL REPORTS

Massachusetts Institute of Technology; Surface Temperatures in a Two-Layer Air-Spaced Slab System Irradiated from One Side; N5ori-07851; NR 051-237.

No. of Copies	Addressee
1	Asst. Chief of Staff, G-2 Department of the Army Washington 25, D. C.
1	Asst. Chief of Staff, G-3 Department of the Army Washington 25, D. C. Attn: Deputy Chief of Staff, G-3, (RR&SW)
1	Asst. Chief of Staff, G-4 Department of the Army, W Washington 25, D. C.
1	Chief of Ordnance Department of the Army Washington 25, D. C. Attn: ORDTX-AR
3	Chief Signal Officer Department of the Army P & C Division Washington 25, D. C. Attn: SIGOP
1	The Surgeon General Department of the Army Washington 25, D. C. Attn: Chairman, Med R&D Board
2	Chief Chemical Officer Department of the Army Washington 25, D. C.
3	Asst. Chief of Engineers for Troop Operations OCE Department of the Army Washington, D. C.
2	The Quartermaster General, CBR, Liaison Office, R&D Div. Department of the Army Washington 25, D. C.

No. of Copies	Addressee
1	Chief of Transportation, Military Planning & Intelligence Department of the Army Washington 25, D. C.
4	Chief, Army Field Forces Fort Monroe, Virginia
1	President, Board #1, OCAFF Ft. Bragg, N. C.
1	President, Board #4, OCAFF Ft. Bliss, Texas
	Commanding General, First Army Governor's Island New York 4, New York
1	Attn: G-1
1	Attn: G-2
1	Attn: G-3
1	Attn: G-4
	Commanding General, Second Army Ft. George G. Meade, Md.
1	Attn: AIAME
1	Attn: AIACM
2	Commanding General, Third Army Ft. McPherson, Georgia Attn: AC ofS, G-3
1	Commanding General, Fourth Army Ft. Sam Houston, Texas Attn: G-3 Section
1	Commanding General, Fifth Army 1660 Hyde Park Blvd. Chicago 15, Illinois Attn: ALFEN
1	Commanding General, Sixth Army Presidio of San Francisco, California Attn: AMGCT-4
2	Commander-In-Chief, FECOM, APO 500 c/o PM San Francisco, California Attn: Ac of S, J-3
1	Commanding General, U. S. Army Alaska APO 942 c/o PM Seattle, Washington

No. of Copies	Addressee
3	Commanding General, US Army Forces Far East (Main) APO 343 c/o PM San Francisco, California Attn: AC of S, G-3
1	Commanding General, US Army Carribean Ft. Amador, C. Z. Attn: Cml O
1	Commanding General, USARFATN & MDPR Ft. Brooke, Puerto Rico
2	Commanding General, US Army Pacific APO 958 c/o PM San Francisco, California Attn: Cml Off
1	Commandant, Command & General Staff College Ft. Leavenworth, Kansas Attn: ALLIS (AS)
1	Commandant, The Artillery School Ft. Sill, Oklahoma
2	Commandant, The Infantry School Ft. Benning, Georgia Attn: CDS
1	Commandant, the AA&GM Branch, The Artillery School Ft. Bliss, Texas
2	Commandant, The Armored School Ft. Know, Kentucky Attn: Class, Doc Sect, Eval & Res Div.
1	Commanding General, Medical Field Service School Brooke Army Medical Center Ft. Sam Houston, Texas
1	Director, Special Weapons Development Office, OCAFF Ft. Bliss, Texas
1	Commandant, Army Medical Service Graduate School Walter Reed Army Medical Center Washington 25, D. C. Attn: Dept. of Biophysics
1	The Superintendent, US Military Academy West Point, New York Attn: Professor of Ordnance

No. of Copies	Addressee
1	Commandant, Chemical Corps School Chemical Corps Training Command Ft. McClellan, Alabama
2	Commanding General, Research & Engineering Command Army Chemical Center, Maryland Attn: Special Projects Officer
2	RD Control Officer Aberdeen Proving Grounds, Maryland Attn: Dir. Ballistics Research Laboratory
3	Commanding General, The Engineer Center Ft. Belvoir, Virginia Attn: Asst. Cmdnt, Eng. School
1	Commanding Officer, Engineer Res. & Dev. Laboratory Ft. Belvoir, Virginia Attn: Chief, Tech Intelligence Branch
1	Commanding Officer, Picatinny Arsenal Dover, New Jersey Attn: ORDBB-TK
1	Commanding Officer, Frankford Arsenal, Ph Philadelphia 37, Pa. Attn: RD Control Officer
1	Commanding Officer, Army Medical Research Laboratory Ft. Knox, Kentucky
2	Commanding Officer, Chemical Corps Chemical and Radiological Laboratory Army Chemical Center, Maryland Attn: Tech. Library
1	Commanding Officer, Transportation R&D Station Ft. Eustis, Virginia
1	Chief, QM R&D Lab., Philadelphia QM Depot 2800 S. 20th St. Philadelphia 45, Pa. Attn: Mr. John Davies, Tech. Library
1	Director, Technical Documents Center Evans Signal Laboratory Belmar, New Jersey
1	Director, Waterways Experiment Station P.O. Box 631 Vicksburg, Miss. Attn: Library

No. of Copies	Addressee
1	Director, Operations Research Office Johns Hopkins University 6410 Connecticut Avenue Chevy Chase, Maryland Attn: Library
2	Chief of Naval Operations Department of the Navy Washington 25, D. C. Attn: OP-36
1	Chief of Naval Operations Department of the Navy Washington 25, D. C. Attn: Op-374 (OEG)
2	Chief, Bureau of Medicine and Surgery Department of the Navy Washington 25, D. C. Attn: Special Weapons Defense Division
1	Chief, Bureau of Ordnance Department of the Navy Washington 25, D. C.
1	Chief of Naval Personnel Department of the Navy Washington 25, D. C. Attn: Pers C
2	Chief, Bureau of Ships Department of the Navy Washington 25, D. C. Attn: Code 348
1	Chief, Bureau of Supplies & Accounts Department of the Navy Washington 25, D. C.
1	Chief, Bureau of Yards & Docks Department of the Navy Washington 25, D. C. Attn: P-312
2	Chief, Bureau of Aeronautics Department of the Navy Washington 25, D. C.
1	Chief of Naval Research, Code 219 Rm 1807, Bldg T-3 Washington 25, D. C. Attn: RD Control Officer

No. of Copies	Addressee
1	Chief of Naval Research, Code 425 Rm 2501, Bldg T-3 Washington 25, D. C. Attn: Chemistry Branch
1	Office of Naval Research Branch Office 150 Causeway St. Boston, Massachusetts
2	Commander-in-Chief, U.S. Atlantic Fleet U. S. Naval Base, Norfolk 11, Virginia
2	Commander-in-Chief, U. S. Pacific Fleet Fleet Post Office, San Francisco,California
4	Commandant, U. S. Marine Corps Washington 25, D. C. Attn: Code A03H
1	President, U. S. Naval War College Newport, Rhode Island
1	Superintendent, U. S. Naval Postgraduate School Monterey, California
2	Commanding Officer, U. S. Naval Schools Command U. S. Naval Station Treasure Island San Francisco, California
	Director, USMC Development Center, USMD Schools Quantico, Virginia
1	Attn: Tactics Board
1	Attn: Equipment Board
2	Commanding Officer, U. S. Fleet Training Center Naval Base, Norfolk 11, Virginia Attn: Special Weapons School
2	Commanding Officer, U. S. Fleet Training Center Naval Station, San Diego 36, California Attn: (SPWP School)
1	Commanding Officer, Air Development Squadron 5, VX-5 U. S. Naval Air Station, Moffett Field, California
1	Commanding Officer, U. S. Naval Damage Control Training Center, Naval Base, Philadelphia 12, Pa. Attn: ABC Defense Course
1	Commanding Officer, U. S. Naval Unit, Chemical Corps School, Army Chemical Training Center Ft. McClellan, Alabama

No. of Copies	Addressee
	Commander, U. S. Naval Ordnance Laboratory White Oak, Maryland Silver Spring 19, Maryland
1	Attn: EE
2	Attn: R
1	Commander U. S. Naval Ordnance Test Station Inyokern, China Lake, California
2	Officer-in-Charge, U. S. Naval Civil Engineering Research & Evaluation Lab, U. S. Naval Construction Bn Center, Port Hueneme, California Attn: Code 753
1	Commanding Officer, U. S. Naval Medical Research Institute, National Naval Medical Center Bethesda 14, Maryland
1	Director, U. S. Naval Research Laboratory Washington 25, D. C.
1	Director, The Material Laboratory New York Naval Shipyard Brooklyn, New York
1	Commanding Officer & Director, U.S.N. Electronics Lab. San Diego, California Attn: Code 210
3	Commanding Officer, U.S.N. Radiological Defense Lab. San Francisco 24, California Attn: Tech. Info. Div.
1	Commanding Officer & Director David Taylor Model Basin Washington 7, D. C. Attn: Library
1	Commander, U. S. N. Air Development Center Johnsville, Pa.
2	Director, Office of Naval Research Branch Office 1000 Geary Street San Francisco, California
1	Officer-in-Charge, U.S.N. Clothing Factory U.S.N. Supply Activities New York 3rd Avenue & 29th Street Brooklyn 32, New York Attn: R&D Div.

No. of Copies	Addressee
1	Commanding Officer, Naval Medical Field Research Lab. Camp Lejeune, N. C.
1	Asst. for Atomic Energy, Hqs, USAF Washington 25, D. C. Attn: DCS/O
1	Asst. For Development Planning, Hqs, USAF Washington 25, D. C.
1	Director of Operations, Hqs, USAF Washington 25, D. C.
1	Director of Operations, Hqs, USAF Washington 25, D. C. Attn: Operations Analysis
1	Director of Plans, Hqs, USAF Washington 25 D. C. Attn: War Plans
1	Directorate of Requirements, Hqs, USAF Washington 25, D. C. Attn: AFDRQ-SA/M
1	Directorate of Research & Development Armament Division, DCS/D, Hqs USAF Washington 25 D. C.
2	Directorate of Intelligence, Hqs, USAF Washington 25, D. C. Attn: AFOIN-1E2
1	The Surgeon General, Hqs, USAF Washington 25, D. C. Attn: Bio. Def. Br.
1	Commander, Far East Air Forces APO 925, c/o PM San Francisco
2	Alaskan Air Command APO 942, c/o PM Seattle, Wash. Attn: AAOTT
1	Commander, Northeast Air Command APO 862, c/o PM New York, N. Y.
1	Commander, Strategic Air Command Offutt AFB, Omaha, Nebraska Attn: Chief Operations Analysis

No. of Copies	Addressee
1	Commander, Tactical Air Command Langley AFB Virginia Attn: Doc Sec Br.
1	Commander, Air Defense Command Ent AFB, Colorado
	Commander, Air Materiel Command Wright-Patterson AFB Dayton, Ohio
2	Attn: MCAIDS
1	Attn: MCSW
1	Commander, Air Training Command Scott AFB Belleville, Illinois Attn: DCS/O GTP
3	Commander, Air Research & Development Command P.O. Box 1395 Baltimore, Md. Attn: RDDN
1	Commander, Air Proving Ground Command Eglin AFB, Florida Attn: AG/TRB
2	Commander, Air University Maxwell AFB, Alabama
2	Commander, Air Command & Staff School Maxwell AFB, Alabama
2	Commander, Flying Training Air Force Waco, Texas Attn: Dir. of Observer Training
1	Commander, Crew Training Air Force Randolph AFB Randolph Field, Texas Attn: DCS/O, 2GTS
1	Commander, Headquarters Technical Training Air Force Gulfport, Miss. Attn: TA & D
2	Commander, Air Force School of Aviation Medicine Randolph AFB, Texas

No. of Copies	Addressee
1	Commander, Wright Air Development Center Wright-Patterson AFB Dayton, Ohio Attn: WC OMSP
1	Commander, AF Cambridge Research Center 230 Albany Street Cambridge 39, Mass. Attn: Atomic Warfare Directorate
1	Attn: CRTSL-2
3	Commander, AF Special Weapons Center Kirtland AFB New Mexico Attn: Tech. Library
1	Commander, USAF Institute of Technology Wright-Patterson AFB Dayton, Ohio Attn: Resident College
2	Commander, Lowry AFB Denver, Colo. Attn: Dept. of Armament Tng.
3	Commander, 1009th Special Weapons Squadron Hqs, USAF, Washington 25, D. C.
2	The RAND Corporation 1700 Main Street Santa Monica, California Attn: Nuclear Energy Division
1	Executive Secretary, Joint Chiefs of Staff Washington 25, D. C.
1	Director, Weapons Systems Evaluation Group, OSD Rm 2E1006, Pentagon Washington 25, D. C.
1	Asst. for Civil Defense, OSD Washington 25, D. C.
1	Chairman, Armed Services Explosives Safety Board DOD, Room 2403, Barton Hall Washington 25, D. C.
1	Executive Secretary, Military Liaison Committee P.O. Box 1614 Washington 25, D. C.

No. of Copies	Addressee
1	U. S. National Military Representative Headquarters SHAPE APO 55, c/o PM New York, N. Y. Attn: Col. J. P. Healy
1	Asst. Secretary of Defense for Research & Development, DOD, Washington 25, D. C. Attn: Tech. Library
1	Commandant, Armed Forces Staff College Norfolk 11, Va. Attn: Secy
6	Commanding General, Field Command AFSWP P.O. Box 5100 Albuquerque, New Mexico
5	ASTIA Document Service Center Knott Building Dayton 2, Ohio
1	Dr. H. C. Hottel Massachusetts Institute of Technology Cambridge 39, Mass.
1	Dr. E. O. Hulbert Naval Research Laboratory Washington 25, D. C.
1	Dr. H. E. Pearse Strong Memorial Hospital 260 Crittenden Blvd. University of Rochester Rochester 7, New York
1	Dr. J. D. Hardy Department of Physiology Cornell University Medical College 1300 York Avenue New York 21, N. Y.
1	Dr. R. P. Peterson Applied Physics Division Sandia Corporation Albuquerque, New Mexico
1	Dr. Alvin C. Graves Los Alamos Scientific Laboratory Box 1663, Los Alamos, New Mexico

No. of Copies	Addressee
1	Dr. Alan R. Moritz or D. A. Axelrod Institute of Pathology 2085 Adelbert Road Cleveland 6, Ohio
1	Dr. Harold Agnew, Director's Office Los Alamos Scientific Laboratory P.O. Box 1663, Los Alamos, New Mexico
1	University of California, Engineering Research P.O. Box 4063, Westwood Village Station Los Angeles 24, California